J. Fluid Mech. (1977), *vol.* 81, *part* 4, *pp.* 657–687
Printed in Great Britain

Further experiments in nearly homogeneous turbulent shear flow

By V. G. HARRIS,† J. A. H. GRAHAM‡ AND S. CORRSIN

Department of Mechanics and Materials Science, The Johns Hopkins University, Baltimore, Maryland 21218

(Received 15 July 1976)

The experiment of Champagne, Harris & Corrsin in generating and studying a nearly homogeneous turbulent shear flow has been extended to larger values of the dimensionless downstream time or strain by the use of a larger mean velocity gradient in the same wind tunnel. The system appears to reach an asymptotic state in which scales and turbulent energy grow monotonically. Two-point covariances and tensor structure of one-point 'Reynolds stress' and 'pressure/strain-rate covariance' agree with the earlier case. However, the linear intercomponent energy exchange hypothesis due to Rotta, very roughly confirmed by the earlier experiment, is contradicted by the present data.

1. Introduction

For reasons mentioned by Champagne, Harris & Corrsin (1970, to be identified as CHC in this paper), especially to avoid the complicating effects of boundaries, it is interesting to study an infinitely extended turbulent shear flow with constant mean velocity gradient. This is unattainable experimentally, but a good approximation to transverse uniformity can be obtained (Rose 1966; CHC 1970; Mulhearn & Luxton 1970, 1975). The reader is referred to CHC for a brief survey of relevant work prior to 1970.

Experimentally, Rose generated a linear turbulent shear flow using a plane grid of parallel rods of uniform diameter and non-uniform spacing. CHC (1970), Rose (1970), Mulhearn & Luxton (1970, 1975) and Hwang (1971) generated shear flows of improved lateral homogeneity with mean strain rates approximately equal to that of Rose (1966).

The purpose of the present experimental study was to generate a higher mean strain rate than that obtained previously, especially to try to attain a larger effective flow development time. A 'paradox' of the first two investigations centred upon the fact that the turbulent energy appeared to reach a steady asymptotic state, while both the integral scales and the microscales exhibited continued growth. Thus although the energy production rate was constant or increasing and the dissipation rate was decreasing, there seemed to be no net increase in turbulent energy.

A resolution of this apparent paradox was suggested in CHC (1970), where it was speculated that the system had not yet reached its asymptotic state. Thus a larger

† Present address: Mechanical Engineering Department, Howard University, Washington, D.C.
‡ Present address: Canadian Pratt & Whitney Co., Longueuil, P.Q.

value of the dimensionless measure of time should find the turbulent energy growing in a fashion consistent with the growing scales.

Ground work as well as ground rules for generating roughly homogeneous turbulent shear flow as found in CHC have been used in the present study to attain a linear mean shear of $d\overline{U}_1/dx_2 = 44\,\mathrm{s}^{-1}$, nearly four times that obtained in the earlier cited work. Keeping the centre-line velocity identical to that in CHC (12·42 m/s), it was anticipated that the effective dimensionless time span available before the downstream end of the test section was reached would be correspondingly extended. This turned out to be the case, and the present work explores and resolves some of the fundamental questions left open by CHC because of a lack of development time, and confirms the suggestion described above.

A still larger effective time could have been attained by lowering the mean speed, but the desire for a larger Reynolds number outweighed that change. Operating at the same speed also maintained negligible downstream boundary-layer effects without a change in the duct-wall configuration.

A preliminary report was presented at a meeting of The American Physical Society (Graham, Harris & Corrsin 1970). As a final comment, on references, we note that the published version (Mulhearn & Luxton 1975) of an earlier unpublished report (Mulhearn & Luxton 1970) omitted all data from the near-asymptotic region, at relatively large dimensionless times. As a consequence, we have used the report rather than the final paper as a source of some comparative data.

2. Analytical preliminaries

Because the experiment to be reported here shows larger downstream inhomogeneity than the earlier case, yet retains the same degree of transverse homogeneity, it is useful to record here the general forms of the velocity moment equations (see, for example, Townsend 1975; or Hinze 1975). The equations for mean mass and momentum balances are too familiar to require repetition of the general forms, but under the restriction of steady rectilinear mean flow, $\overline{U}_2 = \overline{U}_3 = 0$, so the mass balance for constant density in this idealized case reduces to

$$\partial\overline{U}_1/\partial x_1 = 0. \tag{2.1}$$

This means, for example, that $\overline{U}_1(x_2)$ is the same at all values of x_1, the co-ordinate in the mean flow direction.

With the added theoretical restrictions that $d\overline{U}_1/dx_2$ is a non-zero constant, that $\partial\overline{U}_1/\partial x_3 = 0$ and that all turbulence moments are transversely homogeneous (i.e. $\partial(^-)/\partial x_2 = \partial(^-)/\partial x_3 = 0$), the mean momentum equations are

$$\partial\overline{P}/\partial x_1 = -\rho\, d(\overline{u_1^2})/dx_1, \tag{2.2}$$

$$\partial\overline{P}/\partial x_2 = -\rho\, d(\overline{u_1 u_2})/dx_1, \tag{2.3}$$

$$\partial\overline{P}/\partial x_3 = 0, \tag{2.4}$$

where $\overline{P}$ is the mean static pressure and ρ is the density.

Integrating (2.2) and (2.3) partially with respect to x_1 and x_2 respectively, we find

$$\overline{P} = -\rho\overline{u_1^2}(x_1) + f_2(x_2), \tag{2.5}$$

$$\overline{P} = -\rho x_2\, \partial(\overline{u_1 u_2})/\partial x_1 + f_1(x_1). \tag{2.6}$$

Comparison of these necessarily equal functions shows that

$$d(\overline{u_1 u_2})/dx_1 = \text{constant} = c_1 \tag{2.7}$$

and that the mean static pressure field has the form

$$\overline{P} = \overline{P}_{\text{ref}} - \rho\overline{u_1^2}(x_1) - \rho c_1 x_2. \tag{2.8}$$

The dependence of $\overline{P}$ on x_1 seems plausible, because it is analogous to its dependence on x_2 in rectilinear channel flow, for which turbulence moments vary with x_2 but are independent of x_1 (see, for example, Laufer 1950). On the other hand, the dependence of $\overline{P}$ on x_2 in the present case seems less precedented.

Equation (2.7) implies that the asymptotic state of this shear turbulence field will entail a linear growth of $|\overline{u_1 u_2}|$. It seems plausible that such an asymptotic state should also display constant local correlation coefficients or moment ratios: in particular, we should expect $\overline{u_1 u_2}/(\overline{u_1^2}\,\overline{u_2^2})^{\frac{1}{2}}$ to be constant (CHC). If this is so, and if $\overline{u_2^2}/\overline{u_1^2}$ = constant it follows that *$\overline{u_1^2}$ and $\overline{u_2^2}$ will also grow linearly with* x_1. Of course, the mean 'force' balance in the x_2 direction on a rectangular fluid volume requires that the x_1 growth of the tangential force on faces normal to x_1 be counteracted by an x_2 difference in the normal force on faces normal to x_2.

If an evolving quasi-asymptotic state exists, it would be expected to have fixed ratios of all three component energies, so we expect $\overline{u_3^2}$ also to grow linearly with x_1.

The general balance equation for the mean flow kinetic energy per unit mass $E \equiv \frac{1}{2}\overline{U}_i\overline{U}_i$ is

$$\frac{\partial E}{\partial t} + \overline{U}_k\frac{\partial E}{\partial x_k} = \overline{u_i u_k}\frac{\partial \overline{U}_i}{\partial x_k} - \frac{\partial}{\partial x_i}(\overline{U}_k\overline{u_i u_k}) - \frac{1}{\rho}\overline{U}_j\frac{\partial \overline{P}}{\partial x_j} + \nu\frac{\partial}{\partial x_i}\left[\overline{U}_k\left(\frac{\partial \overline{U}_i}{\partial x_k} + \frac{\partial \overline{U}_k}{\partial x_i}\right)\right] - \nu\frac{\partial \overline{U}_i}{\partial x_k}\left(\frac{\partial \overline{U}_i}{\partial x_k} + \frac{\partial \overline{U}_k}{\partial x_i}\right). \tag{2.9}$$

Terms not physically described in CHC are the second, which is the mean flow convection of mean flow kinetic energy, the fifth, which is the mean pressure-gradient work rate, the sixth, which is the energy increase due to the viscous work rate, and the seventh, which is the dissipation rate.

For rectilinear homogeneous shear flow, (2.9) reduces to equation (2.3) of CHC. For steady rectilinear shear flow with a fixed mean velocity gradient $d\overline{U}_1/dx_2$, plus postulated transverse homogeneity but possible downstream changes in turbulence properties (nearly the experimental case), (2.9) reduces at once to

$$0 = \overline{u_1 u_2}\frac{d\overline{U}_1}{dx_2} - \frac{\partial}{\partial x_2}(\overline{U}_1\overline{u_1 u_2}) - \frac{\partial}{\partial x_1}(\overline{U}_1\overline{u_1^2}) - \frac{\overline{U}_1}{\rho}\frac{\partial \overline{P}}{\partial x_1} + \nu\frac{d^2E}{dx_2^2} - \nu\left(\frac{d\overline{U}_1}{dx_2}\right)^2. \tag{2.10}$$

It turns out that these terms just cancel each other in pairs. Because (by postulate) $\partial(\overline{u_1 u_2})/\partial x_2 = 0$, the loss to turbulent energy is exactly balanced by the turbulent transport of E in the $-x_2$ direction. By virtue of (2.2), the pressure-gradient work rate term is exactly balanced by the turbulent transport of E in the x_1 direction (which happens to be the work rate due to the 'Reynolds pressure'). Finally, the rate of viscous transport of E down the E gradient exactly cancels the direct viscous dissipation rate, so (2.10) degenerates to $0 = 0$.

The turbulent energy equation (Reynolds 1895; see, for example, Rotta 1962) reduces to

$$\overline{U}_1 \frac{\partial \bar{e}}{\partial x_1} = -\overline{u_1 u_2}\frac{d\overline{U}_1}{dx_2} - \frac{\partial}{\partial x_1}(\overline{u_1 e}) - \frac{1}{\rho}\frac{\partial}{\partial x_1}(\overline{u_1 p}) + \nu \frac{\partial^2}{\partial x_1^2}(\bar{e} + \overline{u_1^2}) - \epsilon. \tag{2.11}$$

Here $e \equiv \frac{1}{2}u_k u_k$, p is the fluctuation in static pressure and

$$\epsilon \equiv \nu \overline{\frac{\partial u_i}{\partial x_k}\left(\frac{\partial u_i}{\partial x_k} + \frac{\partial u_k}{\partial x_i}\right)}$$

is the mean turbulent dissipation rate. Under the postulated restriction that all turbulence moments (including dissipation) are independent of x_2 and x_3, we have taken

$$\frac{\partial}{\partial x_2}(\overline{u_2 e}) = \frac{\partial}{\partial x_3}(\overline{u_3 e}) = \frac{\partial}{\partial x_2}(\overline{u_2 p}) = \frac{\partial}{\partial x_3}(\overline{u_3 p}) = 0.$$

It is immediately clear that (2.11) is not a proper equation because the left side depends on x_2 (and possibly on x_1) while (by postulate) no terms on the right side depend on x_2. The inevitable conclusion is that a flow of the type postulated in this analysis (steady rectilinear mean flow with constant velocity gradient $d\overline{U}_1/dx_2$, plus transverse homogeneity of turbulence moments) is *impossible*. The stationary flow cannot be homogeneous, not even transversely.†

A qualitative explanation can be extracted from comparison of the energy downwind histories in neighbouring x_1, x_3 slabs of fluid. Suppose that exact transverse homogeneity exists at $x_1 = x_{10}$, so that (2.11) is valid locally. Write (2.11) in the form

$$\frac{\partial \bar{e}}{\partial x_1} = \frac{1}{\overline{U}_1(x_2)}\{\mathscr{P} + \mathscr{T}_1 - \epsilon\}, \tag{2.11a}$$

where $\mathscr{P}$ (energy production rate), τ_1 (turbulent transport rate parallel to x_1) and ϵ (dissipation rate) are 'initially' (i.e. at $x_1 = x_{10}$) independent of x_2. Clearly it is the x_2 dependence of the mean flow convection speed $\overline{U}_1$ which tends to destroy the lateral homogeneity.

In order to estimate the seriousness of this effect in the present case (from the CHC data we see that it was negligible at the smaller strain rate), we consider a 'worst' hypothetical case, in which $\mathscr{P}$ dominates the right side of (2.11a). Then

$$\frac{\partial \bar{e}}{\partial x_1} \approx \frac{-\overline{u_1 u_2}\, d\overline{U}_1/dx_2}{\overline{U}_1(x_2)} \tag{2.12}$$

with the assumed upstream condition $\bar{e}(x_{10}, x_2) = \bar{e}_0 = \text{constant}$. Assuming that the field is sufficiently well developed to allow the proportionality

$$-\overline{u_1 u_2} = A\,\bar{e} \quad (A = \text{constant}), \tag{2.13}$$

(2.12) becomes

$$\frac{\partial \bar{e}}{\partial x_1} \approx \frac{A}{\overline{U}(x_2)}\frac{d\overline{U}_1}{dx_2}\bar{e}. \tag{2.14}$$

† It is instructive at this point to recall the complementary conclusion reached earlier (CHC 1970) that a perfectly homogeneous shear flow cannot be stationary in time.

For each fixed x_2, we integrate 'partially' with respect to x_1, obtaining

$$\bar{e}(x_1, x_2) \approx \bar{e}_0 \exp\left[\frac{A(d\bar{U}_1/dx_2)(x_1 - x_{10})}{\bar{U}_1(x_2)}\right], \tag{2.15}$$

which neglects transport in the x_2 direction. The 'function of integration' is zero.

In order to estimate how far downstream from x_{10} the transverse energy gradient may become appreciable, we compute where it reaches equality with the streamwise gradient. Forming $\partial\bar{e}/\partial x_2$ from (2.15), we find

$$\frac{|\partial\bar{e}/\partial x_2|}{|\partial\bar{e}/\partial x_1|} \approx \frac{x_1 - x_{10}}{\bar{U}_1(x_2)} \frac{d\bar{U}_1}{dx_2}. \tag{2.16}$$

Thus the transverse gradient would grow to be the same order as the streamwise one at a distance

$$x_1 - x_{10} \approx \bar{U}_1 \Big/ \frac{d\bar{U}_1}{dx_2} \tag{2.17}$$

downstream of a transversely homogeneous position. In the present experiment this is roughly 30 cm (compared with turbulence integral scales of order 2–4 cm).

Our inferences are (*a*) that a turbulent shear flow which satisfies (2.11) exactly cannot exist and (*b*) that at least the x_2 transport terms must be restored if the x_1 terms are kept; i.e. instead of (2.11), we must use

$$\begin{aligned}\bar{U}_1 \frac{\partial\bar{e}}{\partial x_1} \approx & -\overline{u_1 u_2}\frac{d\bar{U}_1}{dx_2} - \frac{\partial}{\partial x_1}(\overline{u_1 e}) - \frac{\partial}{\partial x_2}(\overline{u_2 e}) - \frac{1}{\rho}\frac{\partial}{\partial x_1}(\overline{u_1 p}) \\ & - \frac{1}{\rho}\frac{\partial}{\partial x_2}(\overline{u_2 p}) + \nu\frac{\partial^2}{\partial x_1^2}(\bar{e} + \overline{u_1^2}) + \nu\frac{\partial^2}{\partial x_2^2}(\bar{e} + \overline{u_2^2}) - \epsilon.\end{aligned} \tag{2.18}$$

We shall see (§ 4.8) that in the experimental flow both turbulent and viscous transport of turbulent energy are negligible. Hence the operative approximate equation is simply

$$\bar{U}_1 \partial\bar{e}/\partial x_1 \approx -\overline{u_1 u_2} d\bar{U}_1/dx_2 - \epsilon. \tag{2.19}$$

Correspondingly, the component energy equations are

$$\bar{U}_1 \frac{\partial\bar{e}_{(1)}}{\partial x_1} \approx -\overline{u_1 u_2}\frac{d\bar{U}_1}{dx_2} + \frac{1}{\rho}\overline{p\frac{\partial u_1}{\partial x_1}} - \epsilon_{(1)}, \tag{2.20}$$

$$\bar{U}_1 \frac{\partial\bar{e}_{(2)}}{\partial x_1} \approx \frac{1}{\rho}\overline{p\frac{\partial u_2}{\partial x_2}} - \epsilon_{(2)}, \tag{2.21}$$

$$\bar{U}_1 \frac{\partial\bar{e}_{(3)}}{\partial x_1} \approx \frac{1}{\rho}\overline{p\frac{\partial u_3}{\partial x_3}} - \epsilon_{(3)}, \tag{2.22}$$

where $e_{(1)} \equiv \frac{1}{2}u_1 u_1$, etc., $\epsilon_{(1)} \equiv \nu\overline{\frac{\partial u_1}{\partial x_k}\left(\frac{\partial u_1}{\partial x_k} + \frac{\partial u_k}{\partial x_1}\right)}$, etc.

To the same approximation, the balance equation for Reynolds shear stress (Chou 1945) is

$$\bar{U}_1 \frac{\partial}{\partial x_1}(-\overline{u_1 u_2}) \approx \overline{u_2^2}\frac{d\bar{U}_1}{dx_2} - \frac{1}{\rho}\overline{p\left(\frac{\partial u_1}{\partial x_2} + \frac{\partial u_2}{\partial x_1}\right)}. \tag{2.23}$$

Here the viscous term is expected to be negligible at large enough Reynolds numbers (CHC 1970).

To extract from the equations of motion some inference about the downstream growth rate of integral scales of the velocity field, we might examine a basic integral-scale equation, e.g. that given by Rotta (1951). In effect, he derived this equation by integrating the two-point velocity covariance equation over all space separations. Inspired by the isotropic case, where the concept is unequivocal, he defined an integral length scale which is a local function of position:

$$L(\mathbf{x},t) \equiv \frac{3\pi}{4\overline{u_k u_k}} \int_0^\infty \frac{\mathscr{E}(k,t;\mathbf{x})}{k}\, dk,$$

where $\mathscr{E}(k,t;\mathbf{x})$ is the 'three-dimensional' spectrum of turbulent kinetic energy, i.e. the spherical-shell integral of the spectral energy density in wavenumber space. k is the magnitude of the wavenumber. A similar differential equation for a growth rate L_1 can be formed by integrating the homogeneous shear-flow correlation equation as given by Reis (1952), Craya (1958) and Burgers & Mitchner (1953). However, there remain terms which are neither measured nor well estimated by existing theory, so that exercise is better left for the future.

3. Experimental apparatus

3.1. *The wind tunnel and shear-turbulence generator*

The shear-turbulence generator employs the same technique as that used at the smaller strain rates (CHC 1970), and the wind tunnel is that used by Rose (1966) and CHC. The shear generator consists of parallel channels of equal width with adjustable internal resistances. The greater mean shear was obtained by using a greater range of screen resistances. Up to four screens spaced 1·9 cm apart were used in each channel. The 12 channels are each 61 cm long, with aluminium walls 0·318 cm thick spaced at 2·54 cm, between their centres. There is a 0·318 cm square splitter rod along the centre-line of each channel exit plane, to reduce the length and time scales of the initial turbulence. Once again the mean velocity gradient was set by trial and error through the arrangement of the numbers and resistances of the screens in each channel. The finest mesh screens had to be mounted on frames under tension in order to ensure that they remained plane.

The increased resistance gradient (compared with the experiment at a smaller strain rate) caused such large streamline slopes upstream of the shear generator that 'droop snoots' had to be added to several of the flat plates in order to prevent leading-edge separation.

A moderate degree of uniformity was attained (see figure 1). The foregoing gave a mean gradient of $44\,\mathrm{s}^{-1}$ (compared with $12{\cdot}9\,\mathrm{s}^{-1}$ in CHC), with a centre-line mean speed of 12·4 m/s, the same as in the earlier case. As before, the turbulence tends towards transverse uniformity as the 'grid-generated' turbulence decays and the 'shear-generated' turbulence dominates. A shear-dominated flow of acceptable transverse homogeneity is attained by $x_1/h = 7{\cdot}0$ (see figures 2 and 3). The interim condition with a minimum in turbulent energy is passed at $x_1/h = 3{\cdot}5$. At the smaller strain rate (CHC), this region occupied the downstream 25% of the test section, being reached at $x_1/h = 8{\cdot}5$. The use of straight-line segments in figures 2(*a*)–(*c*) represents only an aid to the eye, not a suggestion of the actual profiles. Since our interest was

in only an asymptotic state, few data were taken in the region $x_1/h < 7{\cdot}5$. These few upstream data (not presented) showed slight residual non-uniformity in $\partial\overline{U}_1/\partial x_2$ at $x_1/h = 3{\cdot}5$, with a section average equal to the downstream value of $44\,\mathrm{s}^{-1}$.

3.2. *Instrumentation*

Initially the mean velocity was measured with an array of Pitot tubes and later, after fine adjustments had been made, with a hot-wire anemometer.

By and large, experimentation was performed with equipment similar to that used in CHC (1970), so the equipment will be described here only briefly. Mean and fluctuating velocities were measured with DISA 55D01 constant-temperature anemometers, together with DISA 55D10 linearizers. As before, calibration was performed in the known flow in the wind-tunnel test section without the shear-turbulence generator. Root-mean-square fluctuating voltages were measured with a DISA 55D35 r.m.s. voltmeter. Transverse-component fluctuations u_2 and u_3 were measured with a standard hot-wire X-array, with sensitivity calibrated by yawing the probe $\pm 5°$ in a plane parallel to the 'X' in the empty wind tunnel. Air temperature was monitored with a thermistor bridge system, and was kept constant enough to avoid the need for corrections in velocity measurements.

Two-probe spatial velocity correlations, both with and without time delay, were measured with a PAR Model 101 Correlator. Correlation print-out was performed by a Hewlett–Packard Pen Chart Recorder. Correlation coefficients for zero time delay were mostly extracted from these graphs by reading the $\tau = 0$ value of the correlation curve as well as the two corresponding autocorrelation values of the signals. Some measurements for zero time delays, however, were performed using the previous arrangement (CHC 1970), which employed a multiplier and integrator. There was no significant disagreement.

The traversing mechanism was the same as that used by CHC (1970), and had been developed by Kellogg (1965). Most of the single-wire probes were made in the laboratory and had a 0·635 cm diameter stainless-steel shaft, with wire supports made of jewellers' broaches encased in Nuweld dental cement. The hot wires were 0·00038 cm tungsten with copper-plated end supports and bare sensing portions 0·1 cm long. For some measurements performed with X-arrays, use was made of DISA gold-plated X-meters.

4. Measurements: homogeneity and downstream development

4.1. *Transverse homogeneity*

Figure 1 presents mean velocity profiles $\overline{U}_1(x_2)$ at three downstream distances x_1 from the turbulent shear flow generator. $h = 12$ in., the height of the (square) test section. The straight lines all correspond to $d\overline{U}_1/dx_2 = 44{\cdot}0\,\mathrm{s}^{-1}$, and demonstrate good constancy of this mean strain rate on the $x_3 = 0$ mid-plane. The departures from this value in planes $x_3 = \pm 3$ in. on either side did not exceed 3 %. The centre-line speed is

$$\overline{U}_c = 12{\cdot}4\,\mathrm{m/s}.$$

Figures 2(*a*)–(*c*) show that the one-point turbulence moments are moderately homogeneous. The lines are drawn merely to connect the data points, not to represent estimated profiles. Departures from homogeneity in the x_3 direction are smaller by a factor of 4. A dynamically important measure of possible non-uniformities over

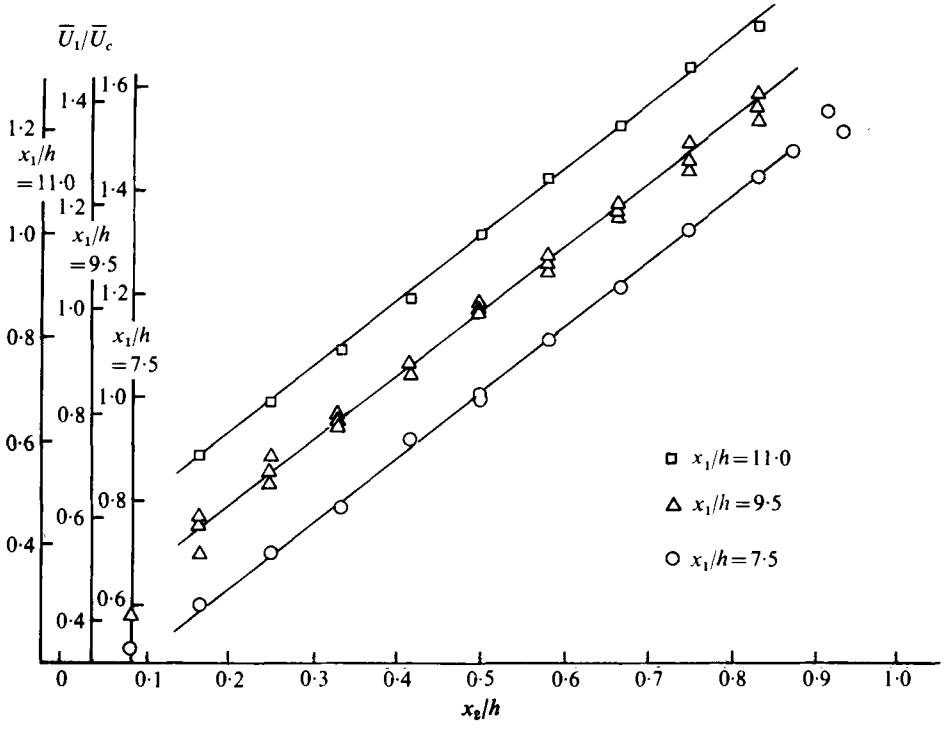

FIGURE 1. Comparison of mean velocity profiles at three downstream stations.

x_3 values is the associated energy production rate $-\overline{u_1 u_3}(\partial \overline{U}_1/\partial x_3)^{-1}$. This was less than 1 % of the dominant production-rate term $-\overline{u_1 u_2}(\partial \overline{U}_1/\partial x_2)^{-1}$. On comparing these profiles with those at the smaller strain rate (CHC 1970, figures 8–10), we note the following.

(*a*) The ratio of the r.m.s. turbulent velocity to the centre-line mean velocity is considerably larger at the larger strain rate: $u_1'/\overline{U}_c$ = 4–5 % here for $7{\cdot}5 \leqslant x_1/h \leqslant 11$, as compared with 1·8 % at the smaller strain rate (CHC, figures 8–10). Since $\overline{U}_c$ cannot be an important parameter far downstream (because after the generation details have been 'forgotten' the field dynamics cannot change under Galilean transformation), it is more appropriate to say simply that the turbulent r.m.s. velocity is larger at the larger strain rate.

(*b*) $\overline{u_1^2} > \overline{u_3^2} > \overline{u_2^2}$ in both cases, but the latter inequality is stronger at the larger strain rate and strain of the present experiment. At $d\overline{U}_1/dx_2 = 44{\cdot}0\,\mathrm{s}^{-1}$ and

$$(x_1/\overline{U}_c)\,d\overline{U}_1/dx_2 = 11{\cdot}9,$$

$\overline{u_3^2}/\overline{u_2^2} = 1{\cdot}46$, whereas at $d\overline{U}_1/dx_2 = 12{\cdot}9\,\mathrm{s}^{-1}$ and $(x_1/\overline{U}_c)\,d\overline{U}_1/dx_2 = 3{\cdot}49$, $\overline{u_3^2}/\overline{u_2^2} = 1{\cdot}17$ (CHC).

(*c*) The Reynolds shear stress correlation coefficient is approximately the same in the two cases ($0{\cdot}47 \leqslant -\overline{u_1 u_2}/u_1' u_2' \leqslant 0{\cdot}50$).

It should be noted also that the small decrease in homogeneity between $x_1/h = 9{\cdot}5$ and 11·0 is in the direction predicted by the discussion in § 2, viz. smaller relative turbulent energies in the faster-moving regions at any constant x_1.

We have too few values to merit the drawing of profile curves, but the degree of

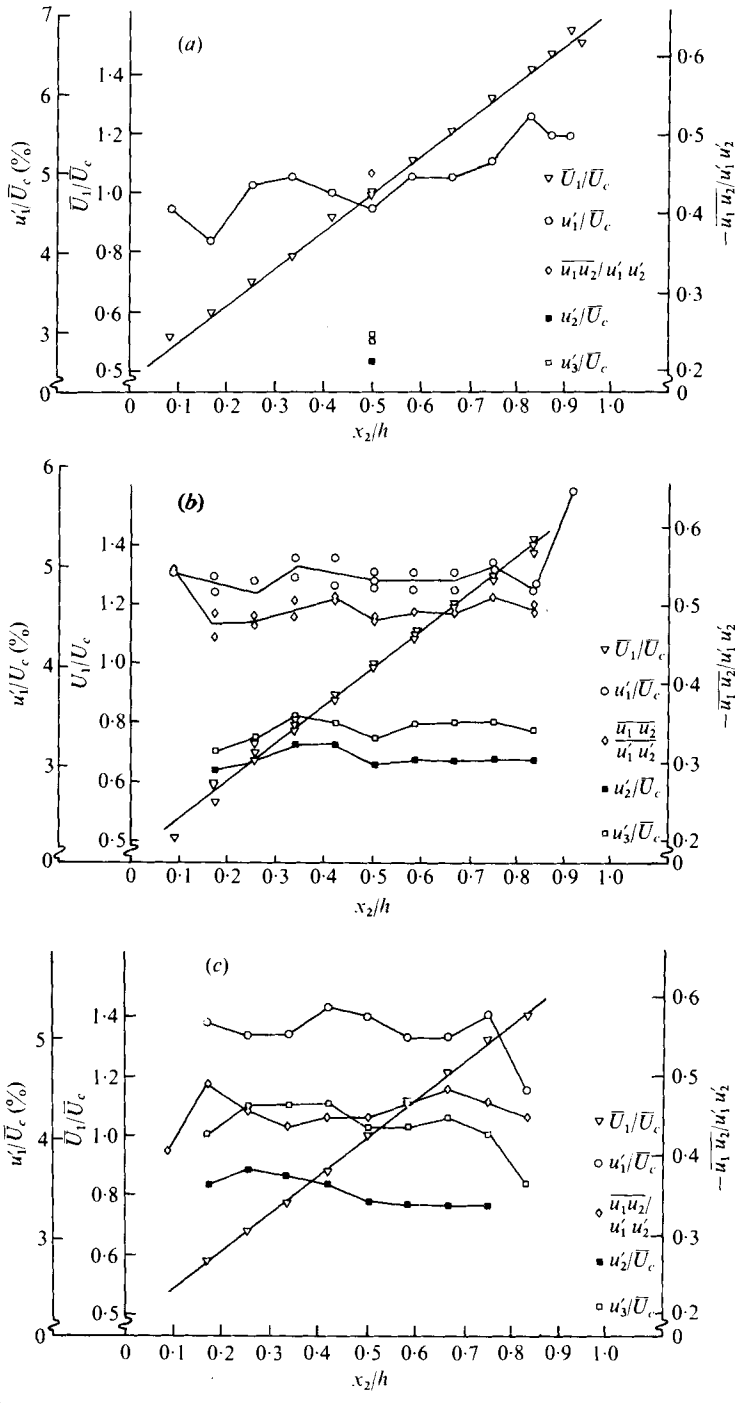

FIGURE 2. Mean velocity and streamwise r.m.s. turbulent velocity profiles at (*a*) $x_1/h = 7{\cdot}5$, (*b*) $x_1/h = 9{\cdot}5$ and (*c*) $x_1/h = 11{\cdot}0$. u_2', u_3' and shear-stress correlation coefficient measured on centre-line only in (*a*), but full profiles in (*b*) and (*c*). $\bar{U}_c = 12{\cdot}9$ m/s is mean velocity on centre-line.

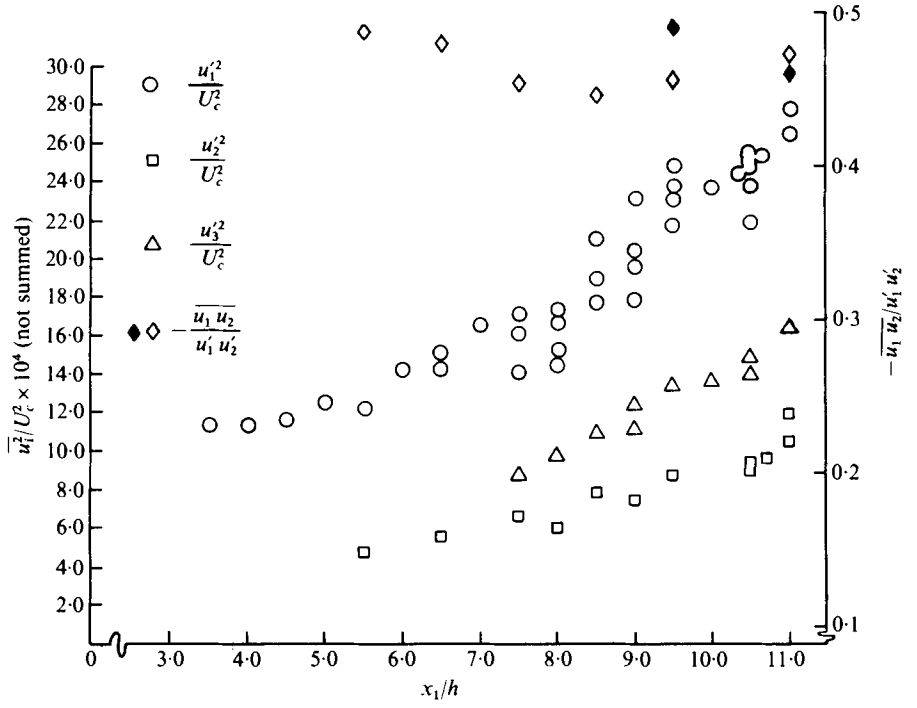

FIGURE 3. Downstream development of turbulence component energies and shear-stress correlation coefficient along tunnel centre-line. ◆, cross-stream averages from figures 2(*b*) and (*c*).

transverse homogeneity of the streamwise integral scale L_1 of the streamwise turbulent velocity u_1 was measured to be $\pm 5\,\%$ over the central half of the airstream. The Taylor microscale λ_1 was about as homogeneous transversely as the r.m.s. turbulent velocities, i.e. within $\pm 5\,\%$.

4.2. *Downstream development*

Figure 3 confirms the expectation (CHC 1970) that, with scales growing in the presence of a constant mean velocity gradient (see figure 4), the magnitudes of the Reynolds-stress components, including the turbulent energy, must grow also. The values of $\overline{u_1 u_2}/u_1' u_2'$, though badly scattered, seem to have attained an asymptotic value well before the turbulent energies. This correlation coefficient is the normalized form of the primary statistical quantity 'added' to the turbulence structure by the mean strain rate, and we hope for a constant asymptotic value. A very weak dependence on the Reynolds number,† which increases with x_1, would not be surprising. Perhaps there is a non-zero asymptotic value of $\overline{u_1 u_2}/u_1' u_2'$ as $R_\lambda \to \infty$; presumably such a value would be approached closely when R_λ is large enough to permit an extensive isotropic inertial subrange in the spectrum (Corrsin 1958; Bradshaw 1967), as postulated by Kolmogorov (1941) and Oboukhov (1941) and confirmed experimentally by a number of investigators (see, for example, Monin & Yaglom 1971, 1975).

Although the data points in figure 5, some recorded as much as two years apart, show considerable scatter, there is a plausible degree of linearity in the downstream growths of all three component energies, a behaviour conjectured in the paragraph preceding (2.9).

† Defined at the end of § 4.4.

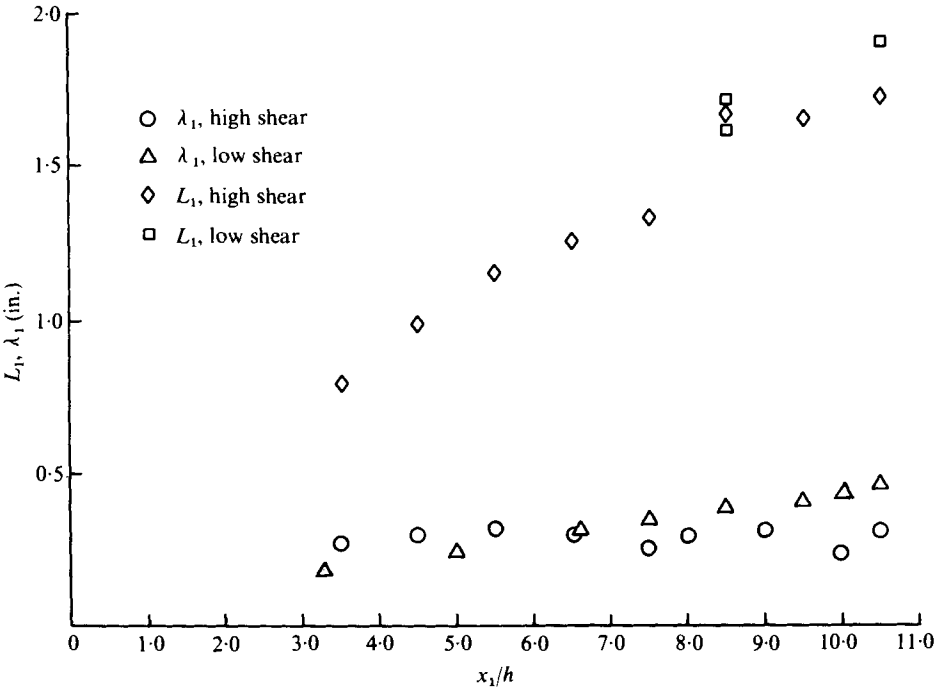

FIGURE 4. Downstream development of 'longitudinal' integral scale and Taylor microscale. Comparison of higher-shear (present) case and lower-shear (CHC) case.

Figure 4 shows that the 'longitudinal' integral scale L_1, inferred from the extrapolated zero-frequency intercept of the one-dimensional spectrum (see, for example, Comte-Bellot & Corrsin 1971, appendix E), continues to grow.

In contrast to the low-shear case, the Taylor microscale (figure 4) shows no downstream growth. It was measured primarily by fitting a vertex-osculating parabola to each temporal autocorrelation curve for u_1, at a fixed space point. With the Taylor approximation,† the autocorrelation for a time interval Δt at a fixed point is very nearly equal to the space correlation for a distance $\Delta x_1 = \overline{U}_1 \Delta t$. The parabola fitting was done on a log plot in the manner of Rose (1966). As partially independent confirmation, some values were measured by differentiating the u_1 signal with respect to time and again invoking the 'Taylor approximation', this time in the form $\partial/\partial t \doteq -\overline{U}_1 \partial/\partial x_1$, for a fixed probe. λ_1 is related to $\partial u_1/\partial x_1$ by Taylor's definition

$$\overline{(\partial u_1/\partial x_1)^2} \equiv 2(\overline{u_1^2}/\lambda_1^2).$$

4.3. *Mean static pressure field*

Equation (2.8) shows that, in the case of a perfectly rectilinear mean flow with exact transverse homogeneity [a condition which cannot be maintained downstream, as we have seen from (2.15)], the mean static pressure will vary with both downstream position and transverse position along the gradient direction. In dimensionless form,

$$\frac{\overline{P}-\overline{P}_{\mathrm{ref}}}{\frac{1}{2}\rho \overline{U}_c^2} = -2\frac{\overline{u_1^2}(x_1)}{\overline{U}_c^2} - \frac{2x_2}{\overline{U}_c^2}\frac{d}{dx_1}(\overline{u_1 u_2}). \tag{4.1}$$

† For more details, see Lumley (1965) and Comte-Bellot & Corrsin (1971, appendix D).

Substituting experimental values for the terms on the right side (table 3, § 4.7),

$$\frac{\overline{P}-\overline{P}_{\text{ref}}}{\frac{1}{2}\rho\overline{U}_c^2} = -5{\cdot}4\times10^{-3}+1{\cdot}9\times10^{-4}\frac{x_2}{h} \quad \text{at} \quad x_1/h = 11{\cdot}0. \tag{4.2}$$

It is evident that the mean static pressure differences should be very small compared with the centre-line dynamic pressure. Readings from static pressure taps on the test-section wall gave order-of-magnitude confirmation. The mean speed on the centre-line was constant over $7{\cdot}5 \leqslant x_1/h \leqslant 11{\cdot}0$, to within the experimental scatter, so the effect of boundary-layer growth was negligible.

4.4. *Accommodation of the low-shear and high-shear cases*

Since the mean strain rate $d\overline{U}_1/dx_2$ is a dimensional quantity, there is, of course, no such thing as a 'low' value or a 'high' value intrinsically. A principal purpose of increasing the value of $d\overline{U}_1/dx_2$ in the experiment was to attain a larger dimensionless development time τ within the same downstream distance x_1 from the generator. We expect that $(d\overline{U}_1/dx_2)^{-1}$ is a characteristic time of the flow,† so

$$\tau \equiv \frac{x_1}{\overline{U}_c}\frac{d\overline{U}_1}{dx_2}, \tag{4.3}$$

where $\overline{U}_c$ is the value of $\overline{U}_1$ on the test-section centre-line. τ represents dimensionless downstream distance and total strain as well.

In order to bring the downstream growth of the mean-square turbulent velocity in figure 3 into consonance with the corresponding property of the low-shear experiment, we should also like to rescale the turbulent energy itself. Using only 'externally imposed' parameters, we can construct a (component) dimensionless energy

$$\frac{q^2}{\overline{U}_c h(d\overline{U}_1/dx_2)}, \tag{4.4}$$

where $q^2 \equiv \overline{u_k u_k}$. This measure, plotted against the dimensionless distance (or time) of (4.3), reconciles the two experiments. However, h ($= 1$ ft) is not a parameter genuinely imposed on the turbulence because the boundary effects are, by design, negligible. In fact, a principal goal of this experiment is to avoid an externally imposed local characteristic scale.‡ Furthermore, $\overline{U}_c$ is not a key velocity measure, as explained earlier, because it is not invariant under Galilean transformation.

Thus a more meaningful scaling of q^2 might be

$$\frac{q^2}{L_1^2(d\overline{U}_1/dx_2)^2}. \tag{4.5}$$

This is plotted on figure 5, where we see the reconciliation of the low-shear and high-shear experiments. It also confirms our conjecture (CHC 1970) that the low-shear experiment had not come very near to an 'asymptotic state' at the downstream end of the wind-tunnel test section; it had just reached a region of minimum energy, where the rate of decay of the generator turbulence has just been balanced by the rate of production due to the general shear.

† For more detailed structure analysis, a combined time which includes both mean and fluctuation effects is doubtless more appropriate [CHC, equation (5.5)].

‡ Of course the generator imposes an initial scale through its slot width, but this merely gives a starting value from which the scale grows freely in the far-downstream, asymptotic region.

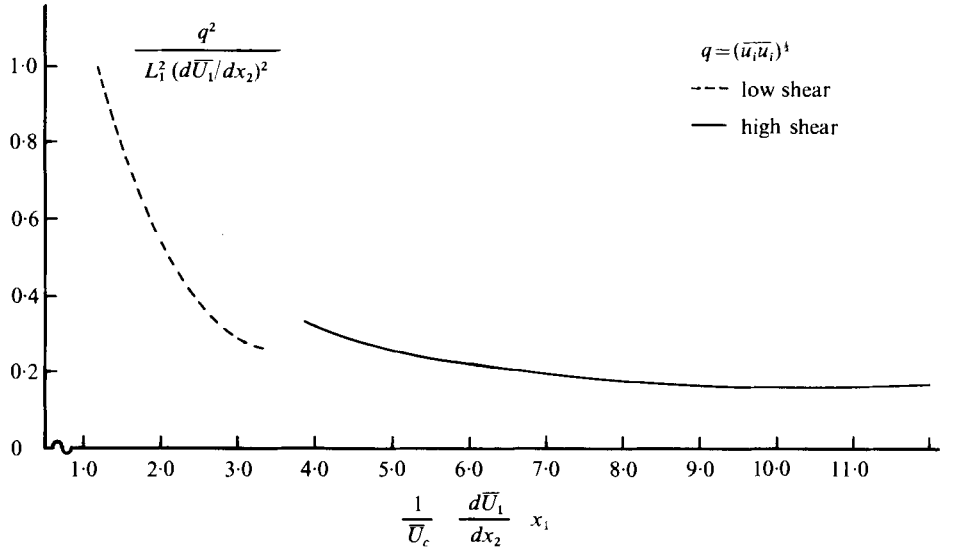

FIGURE 5. Reconciliation of downstream development of turbulent energy in high- and low-shear (CHC) experiments. Abscissa is total strain measured from exit of shear generator.

The L_1 *vs.* x_1/h behaviour (figure 4) evidently needs no rescaling to reconcile approximately the low-shear and high-shear cases. Accepting the idea that the generator 'mesh size' imposes the same initial values on the integral scales in the two cases, should we be surprised that the growth rate of the integral scale seems to be independent of the mean strain rate, although the energy level (and presumably the energy growth rate) depends on it? Indeed the result (which may be only approximate; some weak dependence on $d\overline{U}_1/dx_2$ may exist) is a little surprising, because the mean straining certainly stretches fluid blobs in the direction of its 'positive' principal axis; on the other hand, it squashes them in the direction perpendicular to this.

Perhaps we may associate the growth of the integral scale with a diffusive process [in a constant-gradient scalar field embedded in isotropic turbulence (Corrsin 1952; Wiskind 1962) this is certainly appropriate]. However, the larger 'turbulent diffusivity (proportional to $u_1' L_1$) in the high-shear case would then give more rapid growth, which is not observed.

As an alternative, a spectral dynamic explanation should be sought: a generalization of a simple model which reproduces Kolmogorov's energy decay and scale growth estimates for isotropic turbulence (Comte-Bellot & Corrsin 1971).

Reconciliation of the behaviour of the Taylor microscale for the two shear flows should be sought via exploration of either the mean-square turbulent vorticity or the mean strain rate. At the larger mean strain rate, however, it is less likely that these quantities can be approximated by their isotropic forms [e.g. equation (2.12) of CHC 1970†]. For example, we may expect the vorticity amplification term $\overline{\omega_1 \omega_2} d\overline{U}_1/dx_2$ to be appreciable. Lacking data on $\overline{\omega_1 \omega_2}$, we must be content with trying to reconcile only the ratios of the Taylor microscale to the integral scale. A dimensionless product which has generally shown less variation than its individual factors is $(\lambda/L) R_\lambda$. For

† Two coefficients are misprinted in the correlation function form there, equation (2.13). For the correct coefficients, see equation (5.5.8) in the monograph of Batchelor (1953).

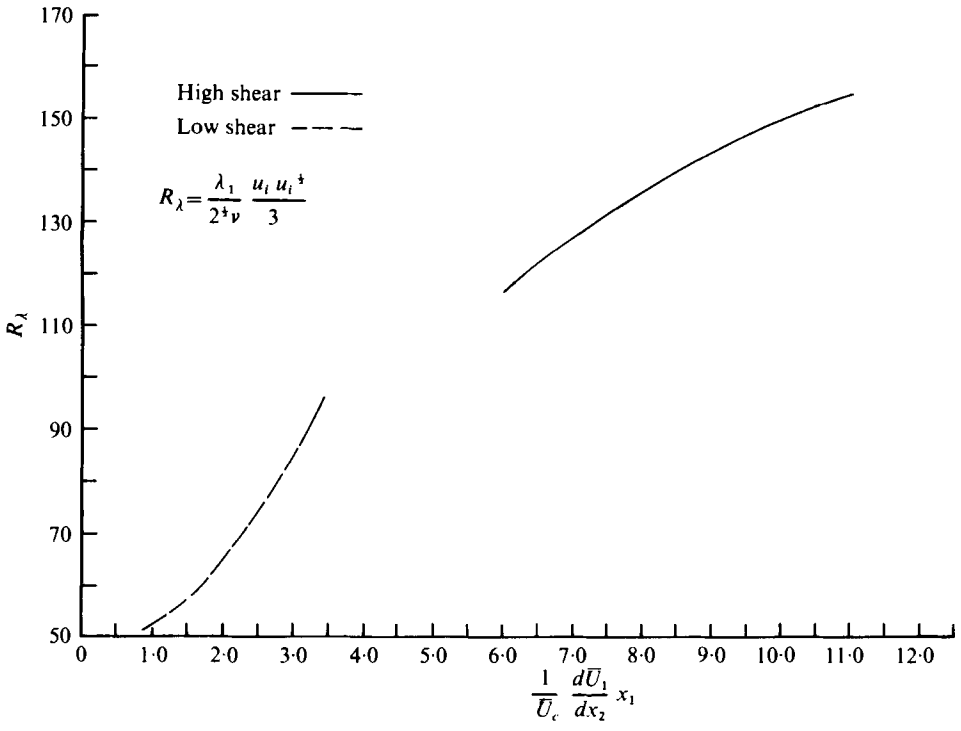

FIGURE 6. Reconciliation of downstream development of turbulence Reynolds number.

isotropic turbulence, the complete similarity assumption of von Kármán & Howarth (1938; for a more complete discussion, see Hinze 1975) predicts that this product is constant during decay; Batchelor (1953, figure 6.1) has shown the approximate empirical constancy of a closely related quantity. More recent experiments on nearly isotropic turbulence (Comte-Bellot & Corrsin 1971) agree.

Even in turbulent shear flows away from boundaries this quantity tends empirically to fall in a range between perhaps 15 and 35. Its relevance in shear flow can be rationalized roughly for cases in which transport of turbulent energy is of secondary importance. If we can assume that the production rate is proportional (though not necessarily equal) to the dissipation rate, and assume isotropic dissipation,

$$-\overline{u_1 u_2}\, d\overline{U}_1/dx_2 \sim \nu(\overline{u_k u_k})^{\frac{1}{2}}/\lambda_1^2. \tag{4.6}$$

Then if $\overline{u_1 u_2} \sim \overline{u_k u_k}$, if $(\overline{u_k u_k})^{\frac{1}{2}} \sim u_1' \sim L_1 d\overline{U}_1/dx_2$† and if the mean-square turbulence components are proportional to each other, (4.6) becomes

$$\lambda_1/L_1 \sim 1/R_{\lambda_1}, \tag{4.7}$$

as in isotropic turbulence. Figure 6 presents the downstream growth of R_λ and figure 7 the product $(\lambda_1/L_1)R_\lambda$ as a function of rescaled downstream distance; neither shows

† Essentially a mixing-length type of proportionality, proposed by Prandtl (1925). Of course the mixing length is more of a Lagrangian scale concept, so we add the assumption that the Eulerian integral scale is proportional to the Lagrangian one.

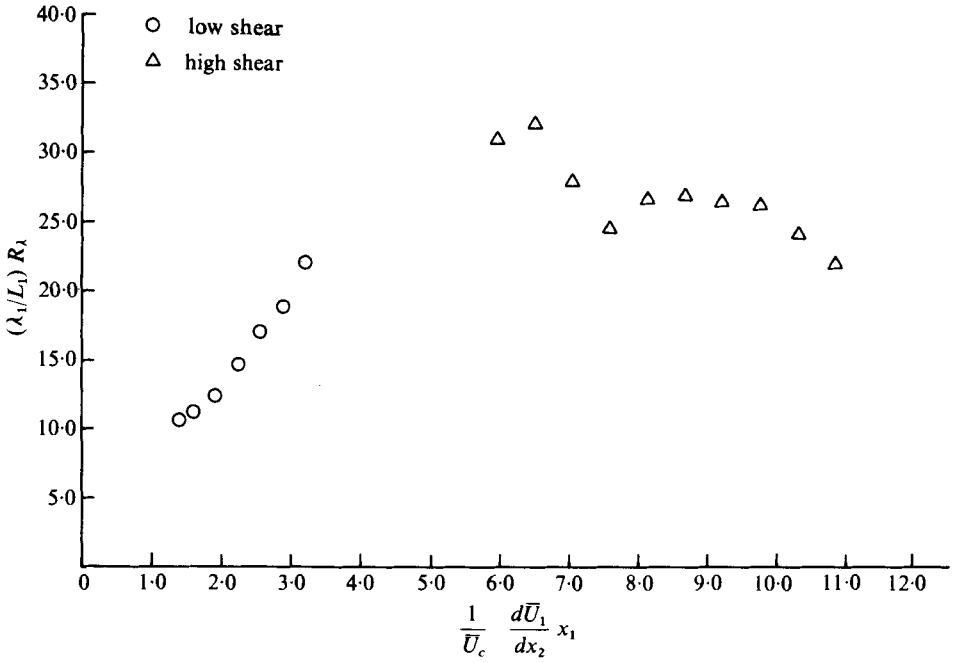

FIGURE 7. Test of a relation sometimes used to estimate the scale ratio.

$\dfrac{dL_1}{dx_1} = 0{\cdot}0148$	$\dfrac{L_1}{\lambda_1}\dfrac{d\lambda_1}{dx_1} = -1{\cdot}2\times10^{-3}$
$\dfrac{L_1}{\overline{u_i u_i}}\dfrac{d\overline{u_k u_k}}{dx_1} = 0{\cdot}0264$	$\dfrac{L_1}{\overline{\lvert u_1 u_2\rvert}/u_1' u_2'}\dfrac{d}{dx_1}\left(\dfrac{\overline{\lvert u_1 u_2\rvert}}{u_1' u_2'}\right) = 1{\cdot}63\times10^{-4}$

TABLE 1

any serious contradiction between the two cases. It is evident here as well as in figure 7 that the data for the small strain rate are all in the development region. Here $R_\lambda \equiv (\lambda/\nu)\,[\frac{1}{3}\overline{u_i u_i}]^{\frac{1}{2}}$. We have assumed the isotropic relation between microscales, viz. $\lambda_1 = 2^{\frac{1}{2}}\lambda$, in computing R_λ.

In the asymptotic region, $(\lambda_1/L_1)\,R_\lambda$ is roughly 25–30, and may be decreasing slowly. To compare this value with that measured for isotropic turbulence [$(\lambda/L)\,R_\lambda \approx 29$, Comte-Bellot & Corrsin 1971] we may also invoke the isotropic integral-scale relation $2L = L_1$. For isotropic turbulence, then, the empirical value is $(\lambda_1/L_1)\,R_\lambda \approx 20$, not too far from the range 25–30 in this shear-flow experiment.

4.5. *Measures of downstream inhomogeneity and of non-stationarity in a convected frame*

Table 1 presents some dimensionless measures of downstream inhomogeneity. Since these are all much smaller than 1·0, we conclude that the spatial homogeneity is good in the downstream direction as well.

In contrast, there is appreciable non-stationarity in a frame translating with the

Choice of T ...	$T = T_{①} = 0{\cdot}0135\,\mathrm{s}$	$T = T_E \approx 0{\cdot}061\,\mathrm{s}$
$\dfrac{TU_c}{L_1}\dfrac{dL_1}{dx_1}$	0·116	0·52
$\left\lvert\dfrac{TU_c}{\lambda_1}\dfrac{d\lambda_1}{dx_1}\right\rvert$	0·0094	0·042
$\dfrac{TU_c}{\overline{u_i u_i}}\dfrac{d\overline{u_i u_i}}{dx_1}$	0·207	0·94
$\left\lvert\dfrac{TU_c}{(\overline{u_1 u_2}/u_1' u_2')}\dfrac{d}{dx_1}\left(\dfrac{\overline{u_1 u_2}}{u_1' u_2'}\right)\right\rvert$	0·0013	0·0059

TABLE 2

centre-line mean speed, as at the smaller shear (CHC 1970). After we have decided upon an appropriate time scale T, we look at stationarity criteria like

$$\left.\begin{gathered}\frac{T\overline{U}_c}{L_1}\frac{dL_1}{dx_1} \ll 1, \quad \frac{T\overline{U}_c}{\lambda_1}\left|\frac{d\lambda_1}{dx_1}\right| \ll 1, \quad \frac{T\overline{U}_c}{\overline{u_k u_k}}\frac{d(\overline{u_i u_i})}{dx_1} \ll 1, \\ \frac{T\overline{U}_c}{|\overline{u_1 u_2}|/u_1' u_2'}\left|\frac{d(|\overline{u_1 u_2}|/u_1' u_2')}{dx_1}\right| \ll 1.\end{gathered}\right\} \tag{4.8}$$

If we select as the characteristic time

$$T_{①} \equiv \left[\frac{1}{L_1}\left(\frac{\overline{u_i u_i}}{3}\right)^{\frac{1}{2}} + \frac{d\overline{U}_1}{dx_2}\right]^{-1} \tag{4.9}$$†

we find at $x_1/h = 11{\cdot}0$ the values in the first column of table 2. The first, second and fourth values are not significantly worse than those in the smaller-shear experiment, which was not 'fully developed' (CHC). But the third shows appreciable departure from stationarity in the turbulent energy.

If we select as the characteristic time the integral time scale of R_{11} in the $\overline{U}_c$-convected frame (the envelope curve of figure 15 extrapolated with a simple exponential function $0{\cdot}665\exp[-0{\cdot}266\,d\overline{U}_1(\Delta t)/dx_2]$), i.e.

$$T_E \equiv \int_0^\infty R_{11}(\overline{U}_c\,\Delta t, 0, 0; x_1, \Delta t)\,d(\Delta t) \quad (\approx 0{\cdot}061\,\mathrm{s\ at}\ x_1/h = 7{\cdot}5), \tag{4.10}$$

we find severe non-stationarity in both the turbulent energy and the integral scale.

It is a bit disconcerting that $T_{①}$ and T_E differ by a factor of 4·5. The inequality prompts us to see whether the basic Eulerian velocity integral time scale T_E is related to the Eulerian velocity and integral length scale in roughly the same proportion as in isotropic turbulence (Comte-Bellot & Corrsin 1971). In (decaying) isotropic turbulence it was found that $[\frac{1}{3}\overline{u_i u_i}]^{\frac{1}{2}}\,T_E/L_1 \approx 1{\cdot}67$. In the present experiment, picking velocity and length scales at the upstream point of the R_{11} measurement, as in the isotropic calculation, gives $[\frac{1}{3}\overline{u_i u_i}]^{\frac{1}{2}}\,T_E/L_1 \approx 1{\cdot}81$, roughly the same value.

Parenthetically, it should be recalled that, if the isotropic turbulence field is rescaled to 'correct' for decay and scale growth, the dimensionless product is 0·78.

† Essentially equation (5.5) of CHC (1970).

4.6. *The intensity or 'strength' of the turbulence*

As remarked earlier, the turbulence level $u_1'/\overline{U}_c$ in this experiment is appreciably larger than that at the smaller shear (CHC), but that cannot be a significant measure of turbulence 'strength' because it changes under a Galilean transformation, which is unacceptable if the boundary and upstream ('initial') conditions are unimportant. The dimensionless ratio plotted in figure 5 is a measure which *is* invariant under Galilean transformation.

In a sense, turbulence Reynolds numbers are measures of vigour. Figure 6 shows the values and downstream growth of a Reynolds number based on the transverse Taylor microscale. The value at the downstream end of the test section is a fairly typical value for a small laboratory experiment.† It is probably insufficient for the existence of an isotropic inertial subrange in the sense of Kolmogorov (1941; see also Corrsin 1957, 1958), and may not even be large enough to permit the use of an isotropic estimate for the viscous dissipation rate. Bradshaw (1967) might disagree. Unfortunately, there has not been sufficient time to measure the degree of local isotropy in detail.

Another measure of the strength of the turbulence in a shear flow is the ratio of its root-mean-square strain rate or vorticity to the corresponding quantity in the mean motion. For comparison with values published earlier (CHC), we use $(\epsilon/\nu)^{\frac{1}{2}}$ as a measure of the r.m.s. strain rate or vorticity, and find at $x_1/h = 11{\cdot}0$

$$\left(\frac{\epsilon}{\nu}\right)^{\frac{1}{2}} \Big/ \frac{d\overline{U}_1}{dx_2} \approx 10{\cdot}2. \tag{4.11}$$

Within the experimental accuracy this is equal to the value of 9·8 measured at the smaller shear.

Still another measure of strength is the ratio of 'turbulent viscosity' to molecular viscosity:

$$\frac{\nu_T}{\nu} \equiv \frac{-\overline{u_1 u_2}}{\nu} \Big/ \frac{d\overline{U}_1}{dx_2} \approx 175, \tag{4.12}$$

which is larger than the value of 90 observed at the smaller shear and is close to the value of 200 computed from turbulent boundary-layer data (Klebanoff 1955; CHC) half-way from the wall to the free stream. It should be reiterated that the (all too common) use of a turbulent viscosity, or some other gradient transport assumption, in the 'classical' turbulent shear flows is wrong in principle because one or more of the following three necessary conditions is normally violated.

(*a*) The length scale of the transporting mechanism must be very small compared with the distance over which the mean value of the property being transported has an appreciable difference in value (Batchelor 1950).

(*b*) The time scale of the transporting mechanism must be very small compared with the characteristic times (if any exist) of the mean fields.

(*c*) For momentum transport, the mean (Reynolds) stress tensor $\{-\overline{u_i u_k}\}$ must have its principal axes parallel to those of the mean strain-rate tensor $\{\partial\overline{U}_i/\partial x_k + \partial\overline{U}_k/\partial x_i\}$ (Corrsin 1957).

† The largest value shown in figure 6 for the small-shear experiment (CHC) is a numerical correction of the value of 130 given in equation (5.7) there. A referee has suggested that u_1' was accidentally used there instead of $\frac{1}{3}\overline{u_k u_k}$. This seems likely.

$\overline{U}_c = 1240\,\mathrm{cm/s}$	$d\overline{U}_1/dx_2 = 44{\cdot}0\,\mathrm{s}^{-1}$
$u_1' = 64{\cdot}1$	$-\overline{u_1 u_2} = 1217\,\mathrm{cm}^2/\mathrm{s}^2$
$u_2' = 40{\cdot}4$	$-\overline{u_1 u_2}/u_1' u_2' = 0{\cdot}47$
$u_3' = 49{\cdot}5$	
$\overline{U}_c\, d\overline{u_1^2}/dx_1 = 1{\cdot}96 \times 10^4\,\mathrm{cm}^2/\mathrm{s}^3$	$L_1 = 2{\cdot}1\,\mathrm{cm}$
$\overline{U}_c\, d\overline{u_2^2}/dx_1 = 0{\cdot}88 \times 10^4$	$\lambda_1 = 0{\cdot}29\,\mathrm{cm}$
$\overline{U}_c\, d\overline{u_3^2}/dx_1 = 1{\cdot}32 \times 10^4$	$dL_1/dx_1 = 0{\cdot}0148$
$-\overline{U}_c\, d(\overline{u\ u_2})/dx_1 = 0{\cdot}62 \times 10^4$	$d\lambda_1/dx_1 = -1{\cdot}07 \times 10^{-4}$
	$\epsilon = 3{\cdot}28 \times 10^4\,\mathrm{cm}^2/\mathrm{s}^3$

TABLE 3

Requirement (*a*) is violated by all traditional turbulent shear flows, although it is satisfied by the deliberately created 'homogeneous' ones (Rose 1966; CHC). Requirement (*b*) is violated by all known turbulent shear flows, including the present one. Requirement (*c*) is roughly satisfied in 'free' shear flows such as jets and wakes but violated in channel and boundary-layer flows (Corrsin 1957) and in homogeneous shear flow (CHC; see also § 5 of this paper).

The fact that analytical gradient-transfer computational models can be forced to give good agreement with experiment for some flow properties (see, for example, Kline *et al.* 1969) in no way confers scientific validity on such assumptions. Furthermore, any empirical confidence such models may engender as pragmatic engineering 'prediction' tools may be proved false with the next unorthodox application.†

4.7. *Turbulent energetics and the mean stress tensor*

It appears that the turbulence has attained an asymptotic state just at the downstream end of the test section, where $\tau \approx 11$–12. Table 3 summarizes some numerical values for this region, estimated from faired curves. Substitution of the appropriate quantities into the approximate form (2.19) of the turbulent energy equation provides an estimate of the turbulent dissipation rate:

$$\epsilon \approx 3{\cdot}28 \times 10^4\,\mathrm{cm}^2/\mathrm{s}^3.$$

An indication of the degree of anisotropy in the dissipative part of the spectrum is given by the contrasting value computed under the assumption of local isotropy:

$$\epsilon_{\mathrm{I}} = 10\,\nu\,\overline{u_k u_k}/\lambda_1^2 \approx 2{\cdot}51 \times 10^4\,\mathrm{cm}^2/\mathrm{s}^3.\ddagger$$

The directions of the principal axes of the mean turbulent (Reynolds) stress tensor $\{-\overline{u_i u_k}\}$ are

$$\alpha_\sigma = \tfrac{1}{2}\tan^{-1}\left[\frac{2\overline{u_1 u_2}}{\overline{u_1^2} - \overline{u_2^2}}\right] = -22{\cdot}3°, 67{\cdot}7°, \tag{4.13}$$

which are very nearly the same as in boundary-layer and channel flow, but quite different from the wake and jet cases (Corrsin 1957). The directions of the principal axes of the mean strain-rate tensor $\{\partial\overline{U}_i/\partial x_k + \partial\overline{U}_k/\partial x_i\}$ are, of course, $\pm 45°$.

† For a more recent and extensive discussion, see Corrsin (1974).

‡ A referee points out that a popular semi-empirical estimator of the dissipation rate, $\epsilon_{\mathrm{II}} = (\frac{1}{3}\overline{u_k u_k})^{\frac{3}{2}}\, L_1$, gives $2{\cdot}67 \times 10^4\,\mathrm{cm}^2/\mathrm{s}^3$.

The two principal stresses in the x_1, x_2 plane are

$$-\sigma_{a,b} = \frac{\overline{u_1^2}+\overline{u_2^2}}{2} \pm \left[\left(\frac{\overline{u_1^2}-\overline{u_2^2}}{2}\right)^2 + (\overline{u_1 u_2})^2\right]^{\frac{1}{2}} = \begin{Bmatrix}4603\\1132\end{Bmatrix} \text{cm}^2/\text{s}^2. \tag{4.14}$$

The third is simply

$$-\sigma_c = -\overline{u_3^2} = 2454\,\text{cm}^2/\text{s}^2. \tag{4.15}$$

The ratio σ_a/σ_b is 4·1, close to values computed from boundary-layer and channel data, namely 3–4 and 3–5 respectively (CHC). This is another indication that the turbulence in this flow is closer to that in traditional shear flows than was the smaller-shear experiment, where $\sigma_a/\sigma_b = 2{\cdot}3$.

4.8. *The pressure/strain-rate tensor*

The component energy equations and shear-stress equation [(2.20)–(2.23)] allow estimation of the physically important tensor

$$P_{ik} \equiv \overline{p(\partial u_i/\partial x_k + \partial u_k/\partial x_i)}. \tag{4.16}$$

Its components give intercomponent energy transfer and destroy shear stress. Unfortunately, there was insufficient time to measure the component dissipation rates, or the viscous term which has been dropped from (2.23). Therefore, in order to estimate (4.16) from (2.20)–(2.23), we just assume local isotropy over the spectral region which governs the second moments of first derivatives (an inaccurate assumption in this experiment, as we saw by comparing ϵ with ϵ_{I}): $\epsilon_{(1)} \approx \epsilon_{(2)} \approx \epsilon_{(3)} \approx \frac{1}{3}\epsilon$. Then (2.20)–(2.23) give component estimates

$$\frac{1}{\rho}\overline{p\frac{\partial u_1}{\partial x_1}} \approx \overline{U}_c \frac{d\bar{\epsilon}_{(1)}}{dx_1} + \overline{u_1 u_2}\frac{d\overline{U}_1}{dx_2} + \frac{\epsilon}{3}, \tag{4.17}$$

$$\frac{1}{\rho}\overline{p\frac{\partial u_2}{\partial x_2}} \approx \overline{U}_c \frac{d\bar{\epsilon}_{(2)}}{dx_1} + \frac{\epsilon}{3}, \tag{4.18}$$

$$\frac{1}{\rho}\overline{p\frac{\partial u_3}{\partial x_3}} \approx \overline{U}_c \frac{d\bar{\epsilon}_{(3)}}{dx_1} + \frac{\epsilon}{3}, \tag{4.19}$$

$$\frac{1}{\rho}\overline{p\left(\frac{\partial u_1}{\partial x_2} + \frac{\partial u_2}{\partial x_1}\right)} \approx \overline{U}_c \frac{d(\overline{u_1 u_2})}{dx_1} + \overline{u_2^2}\frac{d\overline{U}_1}{dx_2}. \tag{4.20}$$

The turbulent transport of turbulent energy (gradients of triple covariance terms) is negligible. For example, from $\overline{u_1^3}$ data (Harris 1974), we estimate the ratio

$$\left|\frac{\partial(\overline{u_1^3})/\partial x_1}{\overline{U}_c\,\partial(\overline{u_1^2})/\partial x_1}\right| < 0{\cdot}03.$$

The viscous transfer of turbulent energy is even smaller, as can be inferred from (4.12).

Then our experimental numerical estimates for the components of the pressure/velocity-gradient tensor are

$$\frac{1}{\rho}P_{ik} \approx 10^4 \begin{Bmatrix} -6{\cdot}56 & 6{\cdot}55 & 0 \\ 6{\cdot}55 & 3{\cdot}06 & 0 \\ 0 & 0 & 3{\cdot}50 \end{Bmatrix} \text{cm}^2/\text{s}^3. \tag{4.21}$$

One principal axis is, of course, in the x_3 direction. Analysing the two-dimensional tensor corresponding to components in the x_1, x_2 plane, we get principal-axis directions

$$\alpha_P \approx -26{\cdot}9°, \quad 63{\cdot}1°, \tag{4.22}$$

which are approximately parallel to the axis of the turbulent stress tensor.

The principal values of $\rho^{-1}P_{ik}$ are

$$\rho^{-1}P_a = -9{\cdot}88 \times 10^4, \quad \rho^{-1}P_b = 6{\cdot}38 \times 10^4, \quad \rho^{-1}P_c = 3{\cdot}50 \times 10^4, \tag{4.23}$$

all in $\mathrm{cm}^2/\mathrm{s}^3$.

4.9. *Test of the linear intercomponent energy transfer hypothesis*

As a first approximation, Rotta (1951, 1962, 1972) suggested that, in the absence of a mean strain rate, the intercomponent energy transfer rate may be simply proportional to the departure from equipartition. In the presence of a mean strain rate, however, the static pressure fluctuation depends in part on this mean motion, and he suggested approximating the resulting additional expression by the value it would have in isotropic turbulence. This rough estimate turns out to give a zero contribution to the intercomponent transfer rates, resulting in a simple linear intercomponent transfer estimate for all turbulent flows.

Formally, the solution of the quasi-Poisson equation for the static pressure fluctuation can be multiplied by the strain-rate fluctuation tensor and averaged (see also Chou 1945):

$$\overline{p\left(\frac{\partial u_i}{\partial x_k}+\frac{\partial u_k}{\partial x_i}\right)} = \frac{\rho}{4\pi}\iiint_\infty \overline{\left(\frac{\partial u_i}{\partial x_k}+\frac{\partial u_k}{\partial x_i}\right)\frac{\partial^2 u_j' u_l'}{\partial y_j \partial y_l}}\,\frac{dV(\mathbf{y})}{|\mathbf{y}-\mathbf{x}|} + \frac{\rho}{2\pi}\iiint_\infty \overline{\left(\frac{\partial u_i}{\partial x_k}+\frac{\partial u_k}{\partial x_i}\right)\frac{\partial u_j'}{\partial y_l}\frac{\partial \bar{U}_l'}{\partial y_j}}\,\frac{dV(\mathbf{y})}{|\mathbf{y}-\mathbf{x}|}, \tag{4.24}$$

$$\mathbf{u} \equiv \mathbf{u}(\mathbf{x}), \quad \mathbf{u}' \equiv \mathbf{u}(\mathbf{y}), \quad \bar{\mathbf{U}}' \equiv \bar{\mathbf{U}}(\mathbf{y}).$$

For this unbounded domain the surface-integral contribution to the solution has been omitted. It is negligible unless the integrand increases without limit at infinity. There is no reason to suppose that this happens.

The first integral in (4.24) arises from the part of the pressure fluctuation which is due solely to self-interaction of the turbulence; the second integral arises from the part of the pressure fluctuation which is influenced by the mean strain rate. For the first integral, which is the entire effect in non-straining flow, Rotta suggested the *ad hoc* form which makes the leading diagonal terms (i.e. the intercomponent energy transfer) simply proportional to the departure from equipartition, i.e.

$$2p\overline{\frac{\partial u_1}{\partial x_1}} = -\rho\epsilon C\frac{\overline{u_1^2}-\frac{1}{3}\overline{u_k u_k}}{\frac{1}{3}\overline{u_i u_i}}, \tag{4.25}$$

with similar forms for $2\overline{p\,\partial u_2/\partial x_2}$ and $2\overline{p\,\partial u_3/\partial x_3}$. Presumably $C > 0$, so that there is a tendency towards energy equipartition.

The tensor form for P_{ik} which reduces to (4.25) for $i = k = 1$ is

$$\overline{p\left(\frac{\partial u_i}{\partial x_k}+\frac{\partial u_k}{\partial x_i}\right)} = -\frac{\rho\epsilon C}{\frac{1}{3}\overline{u_m u_m}}\left(\overline{u_i u_k}-\delta_{ik}\cdot\tfrac{1}{3}\overline{u_j u_j}\right) \tag{4.26}$$

as proposed by Rotta. This gives an explicit form for the off-diagonal components (which destroy turbulent shear stresses), without the need for explicit physical speculation about their actual mechanisms.

For a homogeneous shear flow, the second integral in (4.24) reduces to

$$-\frac{\rho}{2\pi}\frac{d\overline{U}_1}{dx_2}\iiint_{\infty}\left[\frac{\partial^2 K_{i2}}{\partial r_k\,\partial r_1}+\frac{\partial^2 K_{k2}}{\partial r_i\,\partial r_1}\right]\frac{dV(\mathbf{r})}{|\mathbf{r}|}, \tag{4.27}$$

where $K_{mn}\equiv\overline{u_m(\mathbf{x})\,u_n(\mathbf{x}+\mathbf{r})}$ and $\mathbf{r}\equiv\mathbf{y}-\mathbf{x}$. Lacking a theoretical estimate of K_{mn} in shear flow, Rotta (1972) suggested estimating (4.27) by using the form of K_{mn} appropriate to isotropic turbulence. Hanjalić & Launder (1972) and Lumley & Khajeh-Nouri (1974) have made more elaborate conjectures. Our goal in this paper, however, is to present and discuss new experimental data, not to test all interesting analytical hypothesis. We limit the comparison to Rotta's, and include that only because it was tested in the first paper in this series (CHC) and was presented too sketchily there, and also because the new data modify our previous conclusions.

When the isotropic (von Kármán & Howarth 1938) form of R_{ik} is substituted into (4.27), it reduces to simply

$$\tfrac{1}{5}\overline{u_j u_j}\frac{d\overline{U}_1}{dx_2}\{1-\delta_{ik}\}, \tag{4.28}\dagger$$

which makes no contribution to the diagonal components of P_{ik}, the intercomponent transfer of energy. It is therefore fair to say that Rotta's hypothesis for the transfer, even in turbulence which is being sheared, is (4.26).

For the present flow, the data in laboratory co-ordinates give (*a*) different values of C for the three turbulent velocity components and (*b*) relatively constant values for C_1 and C_2 (at differing x_1), but a widely varying value of C_3. We find

$$\left.\begin{aligned} C_1 \approx 2{\cdot}0, \quad C_2 \approx 1{\cdot}2, \\ C_3 \text{ highly variable, ranging from 4 to 12 in the region } 8 < x_1/h < 11. \end{aligned}\right\} \tag{4.29}$$

These depart from each other considerably more than the corresponding quantities in the smaller-shear experiment (CHC): 1·5, 1·2 and 2·0. Presumably the values in (4.29) are more typical of fully developed turbulent flows so we conclude, in contrast to the earlier tentative inference, that the linear intercomponent energy transfer hypothesis is unlikely to be even a fair approximation. The uncertainty in C_3 is discussed below.

To complete the test, we can inspect the equations analogous to (4.26) in principal-axis co-ordinates, ignoring the small misalignment between the axes of $-\overline{u_i u_k}$ and P_{ik}. In principal-axis co-ordinates, the three ratios are $C_a \approx 2{\cdot}2$, $C_b \approx 1{\cdot}4$ and $C_c = C_3$, which approximately follow the trend in laboratory co-ordinates.

Since the variability of the C's indicates serious departure from linearity in the intercomponent energy transfer rate, we might seek an empirical *nonlinear* dependence. Figure 8 displays the component energy gain rate as a function of energy deficiency, the functions on the left and right sides of the three component equations like (4.25). The data of the present experiment are supplemented by those for the weaker-shear case (CHC). The dashed line gives the results of Uberoi's (1957) data on the return

† Although this is not proper tensor notation, it seems clear. $\{1-\delta_{ik}\}$ is zero when $i=k$ and unity when $i\neq k$.

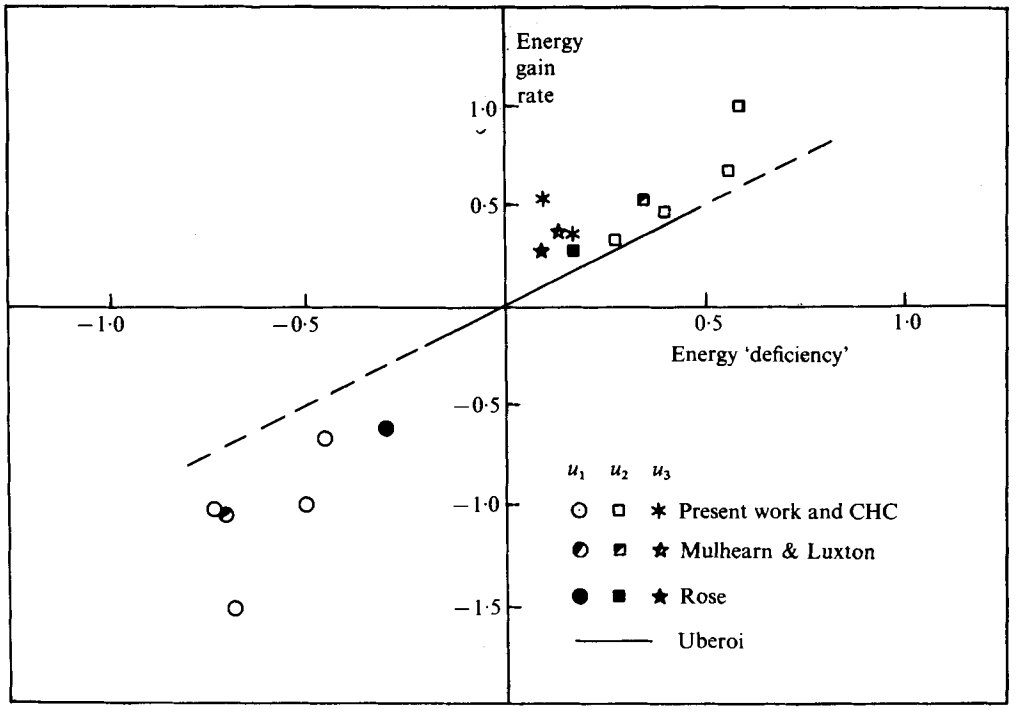

FIGURE 8. Test of Rotta's linear intercomponent energy transfer hypothesis. The energy gain rate is $(\rho\epsilon)^{-1}\,\overline{p\,\partial u_j/\partial x_j}$ (j not summed); the energy 'deficiency' is $(\frac{1}{3}\overline{u_i u_i})^{-1}\,[\frac{1}{3}\overline{u_k u_k} - \overline{u_j^2}]$ (j not summed).

towards isotropy of previously irrotationally strained grid turbulence, as computed by Rotta (1962). From this figure we see that the energy transfer rates to and from $\overline{u_2^2}$ and $\overline{u_1^2}$ (respectively) fall along a reasonably monotonic curve which can roughly include Uberoi's unsheared data. The transfer rate to $\overline{u_3^2}$, however, lies appreciably off this curve. Again, as in CHC, we recall the strange differences between $\overline{u_2^2}$ and $\overline{u_3^2}$ computed by Deissler (1961) and Fox (1964) for homogeneous shear flow at small Reynolds number, by means of the covariance discard hypothesis. They discarded triple velocity covariances but kept pressure–velocity covariances in suddenly sheared isotropic turbulence. Their calculations give a healthy energy transfer from $\overline{u_1^2}$ (and $\overline{u_2^2}$?) to $\overline{u_3^2}$, but lack adequate transfer to $\overline{u_2^2}$, with the result that $\overline{u_2^2}$ dies out an order of magnitude more rapidly than the others.

An inevitable conclusion is that the intercomponent energy transfers to $\overline{u_3^2}$ (the component normal to both mean flow and gradient) and to $\overline{u_2^2}$ (the component along the mean velocity gradient) are qualitatively different.† This suggests that a primary goal of turbulent shear flow theories must be to account for the difference between these two intercomponent transfer rates. This suggests also that we should not expect a simple nonlinear dependence of $\overline{p\,\partial u_i/\partial x_i}$ ($i = 1$ or 2 or 3, not summed) upon

$$(\overline{u_i^2} - \tfrac{1}{3}\overline{u_k u_k})/\tfrac{1}{3}\overline{u_j u_j}$$

† It is, of course, not particularly surprising that $\overline{u_1^2}$ is larger than both $\overline{u_2^2}$ and $\overline{u_3^2}$, because the energy is fed into $\overline{u_1^2}$ from the mean flow kinetic energy (Corrsin 1957).

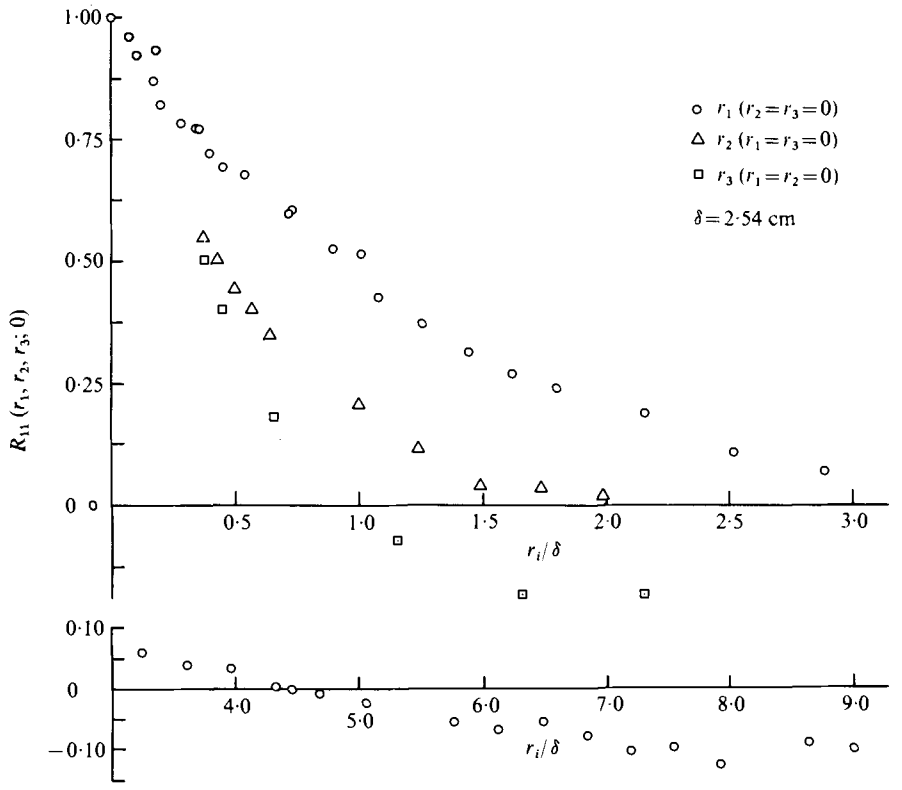

FIGURE 9. Two-point correlation coefficients of u_1 along the three Cartesian axes.

(i not summed), except perhaps in the special case of unsheared turbulence. We shall expect the eventual explanation to possess at least two distinct parts, one reflecting a general tendency towards equipartition without regard for the mean velocity gradient field, the other a model of the different energy absorption by the deficient components along and normal to the gradient.

5. Measurements: two-space-point correlations of velocities

5.1. *Autocorrelation*

Figure 9 presents data on the two-space-point autocorrelation coefficient function $R_{11}(x_1; r_{11} r_2, r_3; 0)$ for the streamwise velocity for $x_1 = 7{\cdot}5\,h$ and $\mathbf{r}$ chosen successively along the three Cartesian co-ordinate directions. Like the corresponding data at smaller shear (and under non-asymptotic conditions, CHC), they show the following characteristic traits which distinguish their relative forms from those typical of isotropic turbulence.

(*a*) The two transverse functions are quite different from each other. $R_{11}(0_1 r_2, 0; 0)$ decreases more slowly, and shows no negative region. $R_{11}(0, 0, r_3; 0)$ reaches a considerable negative value, as it must in order that mass flow be conserved in the 'correlation plane' $(0, r_2, r_3)$.

(*b*) $R_{11}(r_1, 0, 0; 0)$ reaches larger negative values than those measured at smaller shear (CHC).

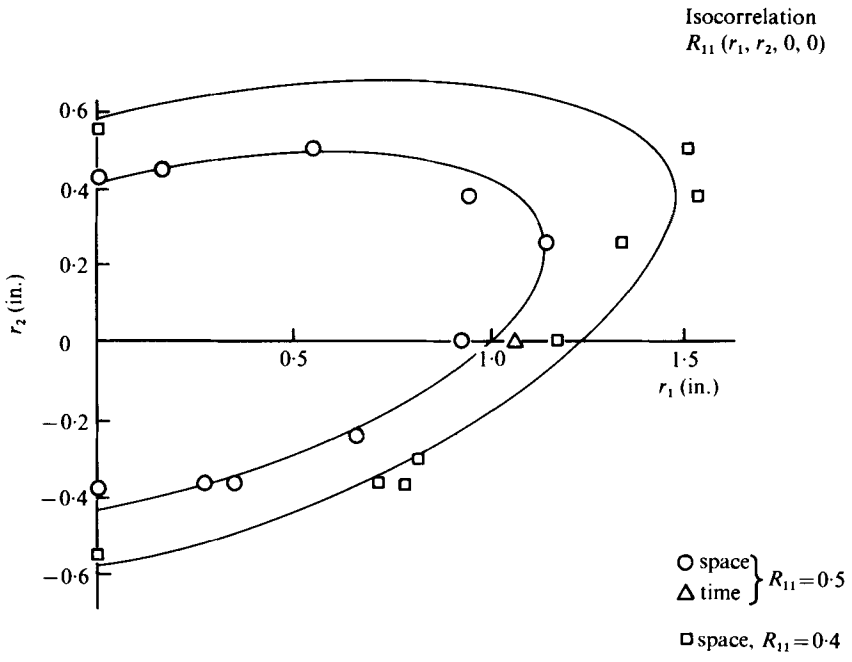

FIGURE 10. Isocorrelation contours of u_1 in the plane containing the flow direction and the gradient direction. The triangle point was measured with a single hot wire and a delayed signal. The top of the $R_{11} = 0{\cdot}4$ contour was sketched to have a familial resemblance.

Possibly typical isocorrelation contours, for $R_{11} = 0{\cdot}5$ and $0{\cdot}4$, are shown in figure 10. Unequivocally they show tilted oval shapes, qualitatively like those in traditional shear flows (see, for example, Sabot & Comte-Bellot 1972). One of the slightly puzzling properties of the smaller-shear case (CHC, figures 25, 44) was the nearly non-existent shear-induced 'distortion' of isocorrelation contours in the r_1, r_2 plane from a form appropriate to isotropic turbulence. If we assume that the unmeasured part of the $R_{11} = 0{\cdot}5$ contour, for $r_1 < 0$ in figure 10, is antisymmetric with that displayed, there is a major axis of approximate symmetry, and it is tilted at about 13° to the x_1 axis.

Figure 11 presents two typical isocorrelation contours in the r_1, r_3 plane. Except for downstream growth effects in x_1, these are presumably symmetric about both the r_3 and the r_1 direction. Configuration details of our probe supports made it inconvenient to measure in the other three quadrants of this plane.

5.2. *Cross-correlation*

Since $-\overline{u_1 u_2}$ is the turbulent shear stress, it is interesting to measure the two-point correlation field $R_{12}(r_1, r_2, r_3; \Delta t)$ of u_1 and u_2. Figure 12 shows the results for zero time delay and space separations along each of the Cartesian axes.

Qualitatively, the three functions are proportioned much like R_{11} (figure 9), showing a considerable negative loop with r_3 separation. In perfectly homogeneous shear, only $R_{12}(0, 0, r_3; 0)$ of these three can be shown *a priori* to be symmetric by reflexion in a Cartesian-axis plane. Therefore we checked the degree of symmetry of $R_{12}(0, r_2, 0; 0)$ along the momentum transfer direction (figure 13). It is symmetric within the precision of the data:

$$R_{12}(0, -r_2, 0; 0) \approx R_{12}(0, r_2, 0; 0). \tag{5.1}$$

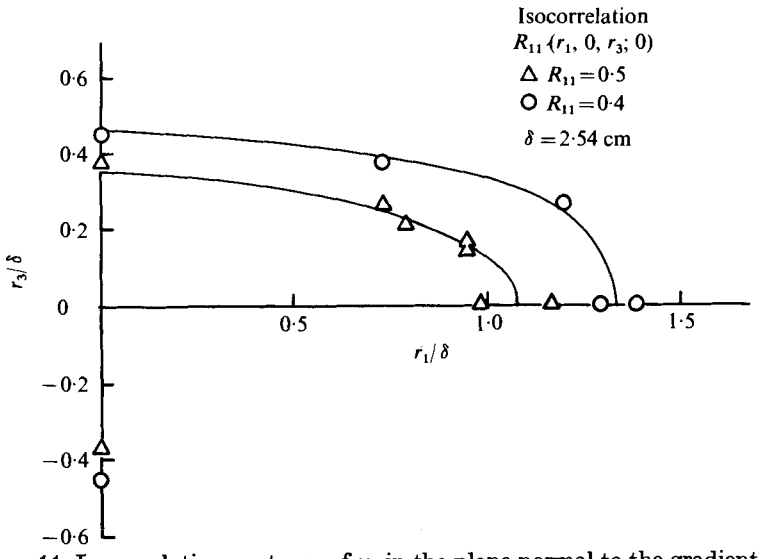

FIGURE 11. Isocorrelation contours of u_1 in the plane normal to the gradient direction.

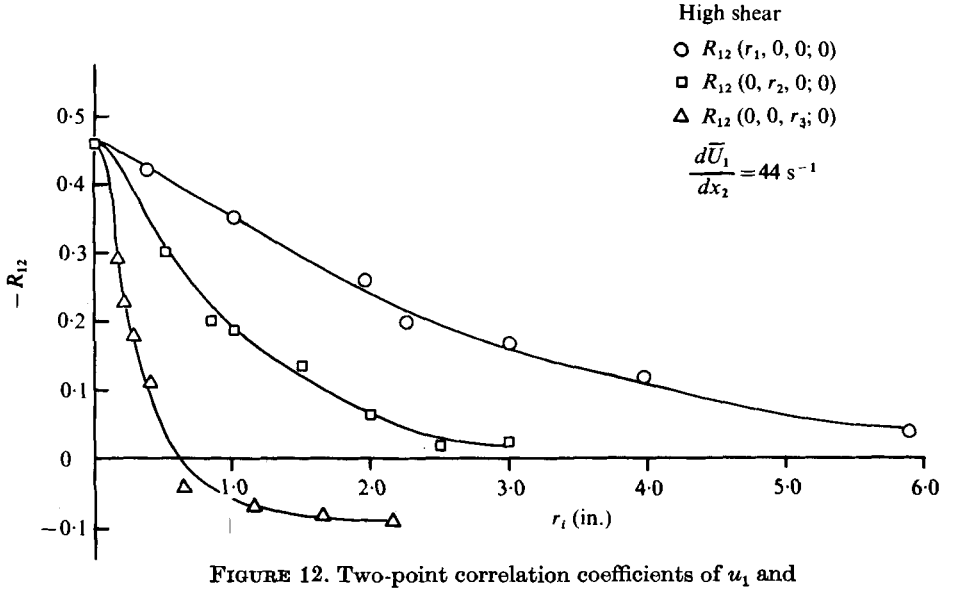

FIGURE 12. Two-point correlation coefficients of u_1 and u_2 along the three Cartesian axes.

We note in passing that the transverse homogeneity of the field makes

$$R_{12}(0, -r_2, 0; 0) = R_{21}(0, r_2, 0; 0). \tag{5.2}$$

The 0·2 isocorrelation contour in two quadrants of the r_1, r_2 plane (figure 14) appears to be a tilted oval, if we assume reflective antisymmetry in the r_2 axis – an assumption which is less plausible for R_{12} than for R_{11}. With this assumption, a rough guess at a 'major axis' gives it a tilt of 16° to the x_1 axis.

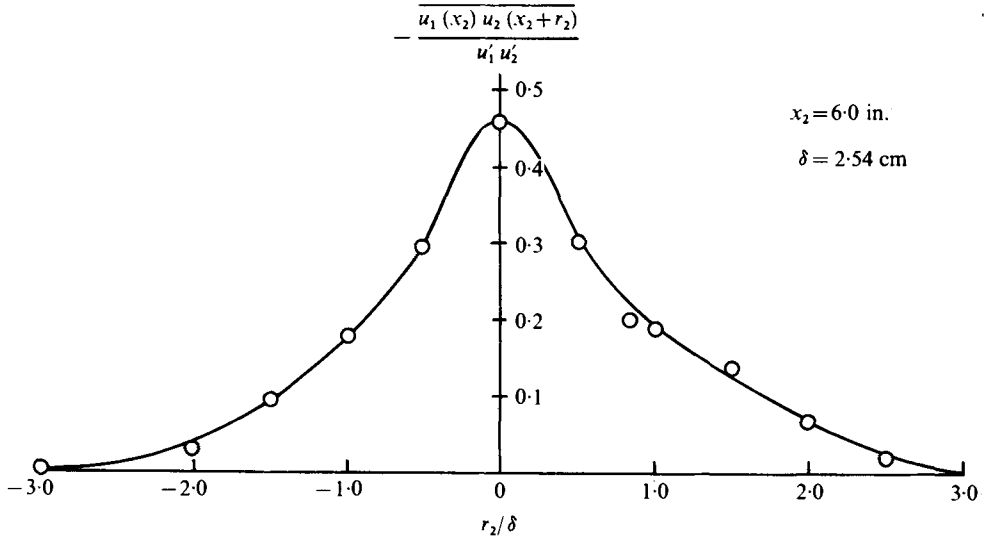

FIGURE 13. A test of the symmetry of $R_{12}(0, r_2, 0; 0)$ along the gradient direction.

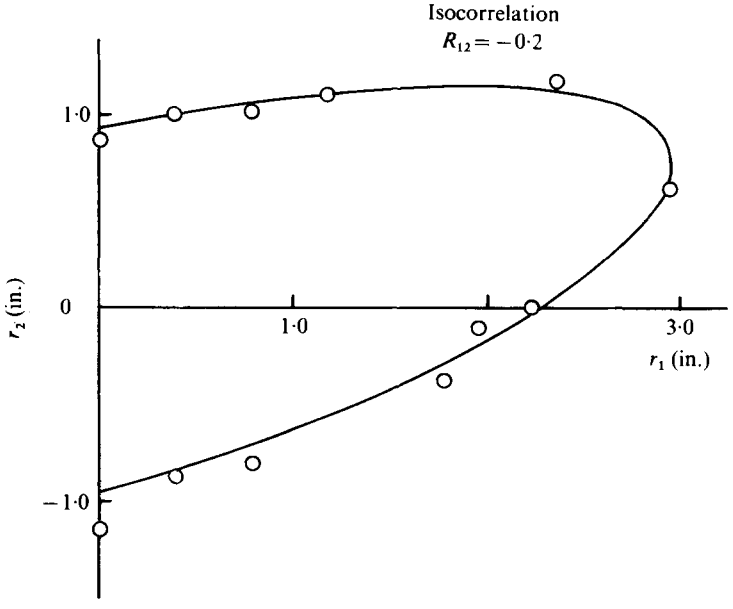

FIGURE 14. Isocorrelation contour of the cross-correlation of u_1 and u_2 in the plane containing the flow direction and the gradient direction.

6. Measurements: space–time correlations of velocities

Especially in transversely homogeneous turbulent flows, the time statistical history in a frame translating with the mean velocity in the fluid layer of interest has a direct significance. In the traditional turbulent shear flows such as boundary layers and jets, curvature of the mean velocity profile prevents simple *a priori* identification of the frame speed which will yield data with the simplest interpretation.

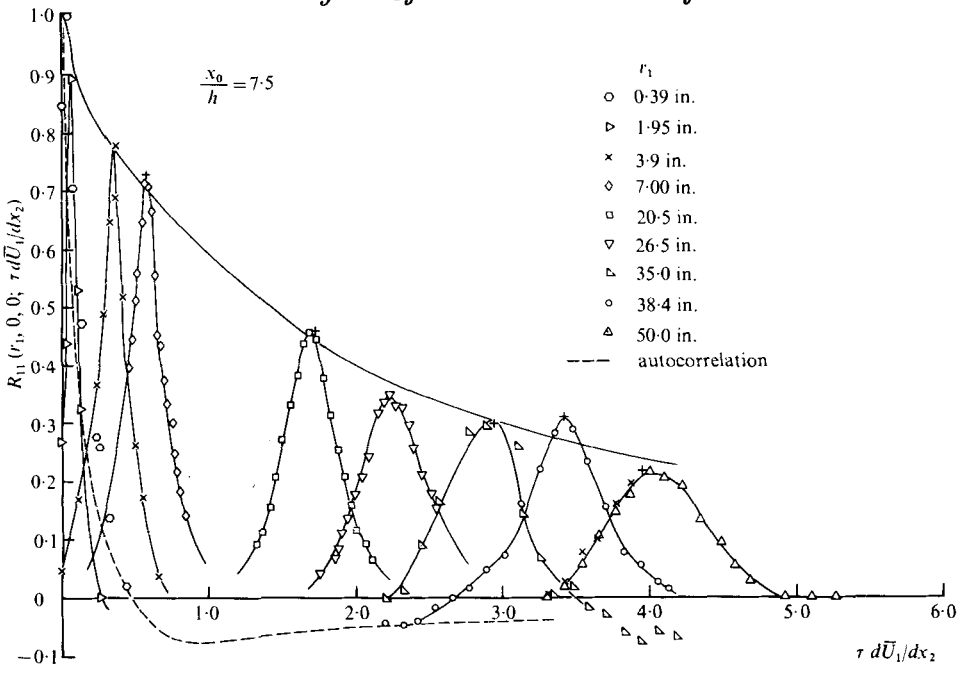

FIGURE 15. Two-point space–time correlation of u_1 velocity, with two probes separated in streamwise direction. +, arrival time corresponding to the mean velocity $\bar{U}_c$.

With two hot-wires probes aligned in the x_1 direction and separated by a distance r_1, we have measured the correlation of curves of

$$R_{11}\left(r_1, 0, 0; \frac{d\bar{U}_1}{dx_2}\Delta t\right)$$

with the upstream wire at $x_1/h = 7{\cdot}5$ (figure 15). This may be compared with figure 22 of CHC, where the maximum attainable value of this dimensionless time delay (when the end of the test section was reached) was only 0·90. Even with the larger strain rate, we still could not attain $R_{11} \ll 1$ within the usable test section.

Figures 16 and 17 show a similar history for R_{22}, which was not pursued as far downstream, and $-R_{12}$, which was. Evidently $(R_{22})_{\max}$ drops off more rapidly with downstream distance than does $(R_{11})_{\max}$; and $(-R_{12})_{\max}$ is the most persistent of the three functions. This is displayed most clearly by the envelopes of the three families of curves (figure 18) when

$$R_{12}\left(r_1, 0, 0; \frac{d\bar{U}_1}{dx_2}\frac{r_1}{\bar{U}_c}\right)$$

is normalized by $R_{12}(0, 0, 0; 0)$.

With the uniform velocity gradient, it is not surprising that the maxima of $R_{ik}(r_1, 0, 0; \Delta t)$ occur essentially at $\Delta t = r_1/\bar{U}_1$.

7. Concluding remarks

Because of the unavoidable downstream growth of transverse inhomogeneity (§ 2), it seems unlikely that this tunnel technique for generating nearly homogeneous turbulent shear flow can be extended much further in terms of the total strain. Fortunately, it appears that a quasi-asymptotic state has been reached. As seems

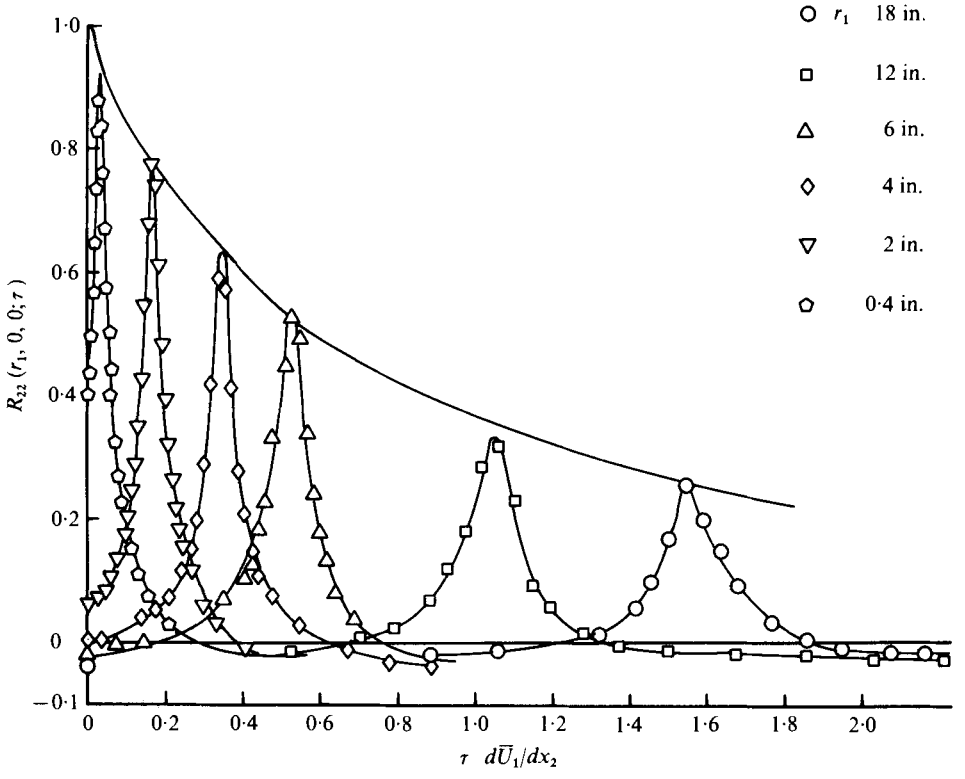

FIGURE 16. Two-point space–time correlation of u_2 velocity, with two probes separated in streamwise direction.

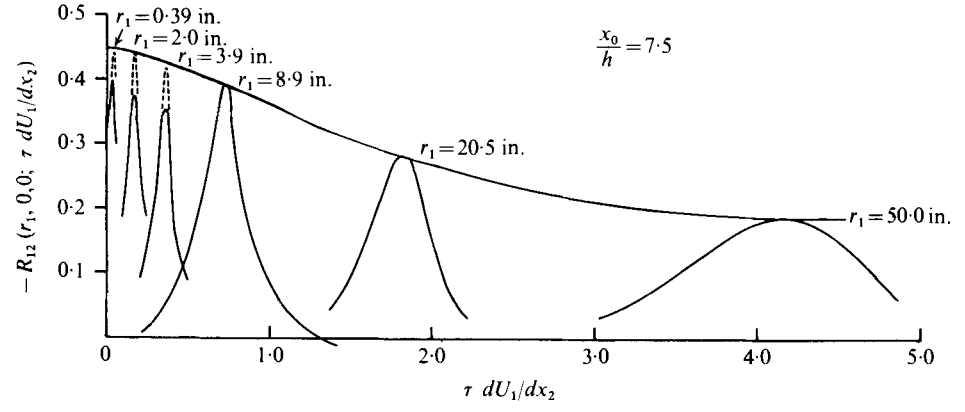

FIGURE 17. Two-point space–time cross-correlation of u_1 and u_2, with two probes separated in streamwise direction. The dashed peaks indicate probe interference correlations required to give the (more accurate) single-probe value for $\tau = 0$.

consistent with the moment differential equations (§ 2), this state is non-stationary in a frame convected with the centre-line mean speed $\bar{U}_c$, with both turbulent energy and integral scales growing. The data indicate that roughly $\overline{u_i u_i} \sim x_1$ and $L_1 \sim x_1$, so the turbulence Reynolds number based on the integral scale $R_{L_1} \equiv (\frac{1}{3}\overline{u_i u_i})^{\frac{1}{2}} L_1/\nu \sim x_1^{\frac{3}{2}}$. This corresponds theoretically to a Taylor microscale growth rate $\lambda \sim x_1^{\frac{1}{2}}$, and $R_\lambda \sim x_1^{\frac{3}{4}}$. The λ_1 data are too scattered to give clear support for the former. The Kolmogorov

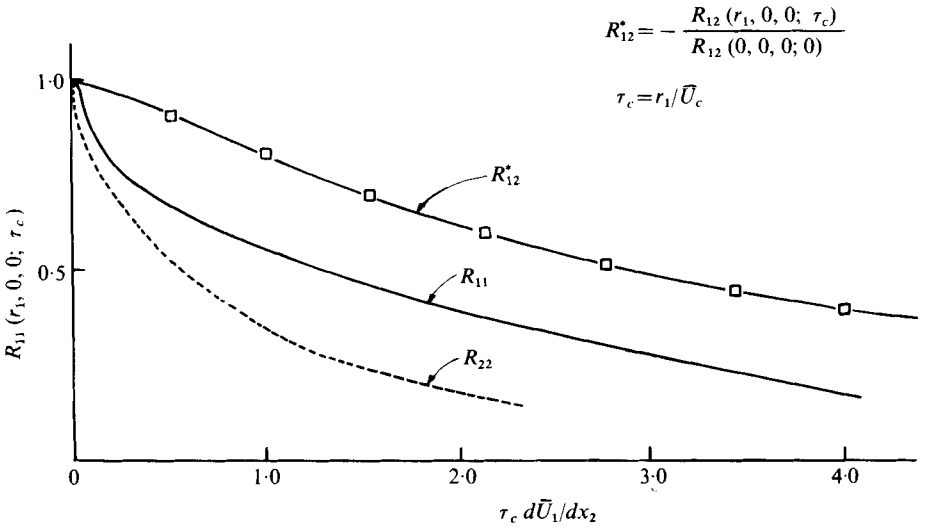

FIGURE 18. Comparison of the envelopes of the space–time correlation functions in figures 15–17, hence the two-time correlation functions in a frame convected with the mean speed $\bar{U}_c$. R_{12} is normalized with its maximum value.

microscale $\eta \equiv (\nu^3/\epsilon)^{\frac{1}{4}}$ can be estimated from $\eta = (15)^{-\frac{1}{4}} R_\lambda^{-\frac{1}{2}} \lambda$, whence $\eta \sim x_1^{-\frac{1}{2}}$, a decreasing quantity.

Because wavelike models surface from time to time in the theoretical turbulence literature (see, for example, Landahl 1967), it is worth emphasizing the fact that in these flows with uniform mean velocity gradients the turbulence structures are merely convected with the gross motion of the fluid. This is in sharp contrast to the commonly accepted notion of a 'wave' as a disturbance which has a characteristic propagation speed *relative* to the material in which it resides. Of course, when a rectilinear mean velocity profile is curved, there is no well-defined choice for 'the mean velocity' of the fluid associated with a turbulent structure (such as the two-point velocity covariance function); this fact alone virtually guarantees that a plausible choice of mean speed of the statistically defined structure will differ from a plausible choice of mean flow velocity for the fluid containing the structure. Such a velocity difference is not by itself evidence of dynamic wavelike behaviour. If wavelike models are to be justified, basic mechanisms for oscillation (especially the 'restoring' forces; high Reynolds number flows have more than enough inertia to provide the necessary 'overshoot' mechanism) should be identified.

Among the simpler attributes of turbulent shear flow which now seem sufficiently characteristic to warrant further study, both experimental and theoretical, are (*a*) the inequalities $\overline{u_1^2} > \overline{u_3^2} > \overline{u_2^2}$, with the related phenomenon of (*b*) 'pathologically' effective transfer of turbulent kinetic energy from $\overline{u_1^2}$ (and/or $\overline{u_2^2}$?) to $\overline{u_3^2}$, (*c*) the prominent negative region in $R_{11}(0, 0, r_3; 0)$, contrasted with the absence of a negative region in $R_{11}(0, r_2, 0; 0)$, (*d*) the orientations of the principal axes of the stress tensor $-\overline{u_i u_k}$ and the pressure/strain-rate tensor $\overline{p(\partial u_i/\partial x_k + \partial u_k/\partial x_i)}$ and (*e*) the orientation of the oval isocorrelation contours of velocity.†

† In an unpublished computational model of homogeneous, *two-dimensional*, turbulent shear flow, we found that the isocorrelation ovals tilted in the opposite direction.

The inequality $\overline{u_3^2} > \overline{u_2^2}$ was observed also at the smaller strain rate and smaller total strain (CHC), but the inequality is especially strong at the larger strain rate:

$$\overline{u_3^2}/\overline{u_2^2} = 1{\cdot}5,$$

here compared with 1·2 in CHC. Such shear-generated inequalities should depend also upon the total strain, preferably measured from a hypothetical isotropic reference state. $(x_1/\overline{U}_c)\, d\overline{U}_1/dx_2$, which is linear in the mean strain, is 3·14 times larger in the present case. Of course the experiment gives no clear choice of effective origin.

This work was supported primarily by the Atomic Energy Commission (Meteorology Branch), more recently by the National Science Foundation (Engineering Mechanics and Atmospheric Sciences Programs). It is based in part upon several sections of the Ph.D. thesis of V. G. Harris (1974). We should like to thank the referees for detecting inconsistencies and points needing clarification.

REFERENCES

BATCHELOR, G. K. 1950 *J. Aero. Sci.* **17**, 441.

BATCHELOR, G. K. 1953 *The Theory of Homogeneous Turbulence*. Cambridge University Press.

BRADSHAW, P. 1967 *Nat. Phys. Lab. Aero. Rep.* no. 1220.

BURGERS, J. M. & MITCHNER, M. 1953 *K. Ned. Akad. V. Wet.* B **15**, 228, 383.

CHAMPAGNE, F. H., HARRIS, V. G. & CORRSIN, S. 1970 *J. Fluid Mech.* **41**, 81.

CHOU, P. Y. 1945 *Quart. Appl. Math.* **3**, 38.

COMTE-BELLOT, G. & CORRSIN, S. 1971 *J. Fluid Mech.* **48**, 273.

CORRSIN, S. 1952 *J. Appl. Phys.* **23**, 113.

CORRSIN, S. 1957 *Proc. 1st Naval Hydr. Symp.* Nat. Acad. Sci./Nat. Res. Counc., Washington, D.C., publ. 515.

CORRSIN, S. 1958 *N.A.C.A. Res. Memo.* RM 58B11.

CORRSIN, S. 1974 *Adv. in Geophys.* A **18**, 25.

CRAYA, A. 1958 *Publ. Sci. Tech. Min. Air*, no. 345.

DEISSLER, R. G. 1961 *Phys. Fluids* **4**, 1187.

FOX, J. 1964 *Phys. Fluids* **7**, 562.

GRAHAM, J. A. H., HARRIS, V. G. & CORRSIN, S. 1970 *Bull. Am. Phys. Soc.* **15**, 1544.

HANJALIĆ, K. & LAUNDER, B. E. 1972 *J. Fluid Mech.* **52**, 609.

HARRIS, V. G. 1974 Ph.D. dissertation, Johns Hopkins University.

HINZE, J. O. 1975 *Turbulence*, 2nd edn. McGraw-Hill.

HWANG, W. S. 1971 Ph.D. dissertation, University of Virginia.

KÁRMÁN, T. VON & HOWARTH, L. 1938 *Proc. Roy. Soc.* A **164**, 192.

KELLOGG, R. M. 1965 Ph.D. dissertation, Johns Hopkins University.

KLEBANOFF, P. 1955 *N.A.C.A. Rep.* no. 1247.

KLINE, S. J., MORKOVIN, M. W., SOVRAN, G. & COCKRELL, D. J. (eds.) 1969 *Computation of Turbulent Boundary Layers*. Dept. Mech. Engng, Stanford University, California.

KOLMOGOROV, A. N. 1941 *C.R. Akad. Sci. S.S.S.R.* **30**, 301.

LANDAHL, M. 1967 *J. Fluid Mech.* **29**, 441.

LAUFER, J. 1950 *J. Aero. Sci.* **17**, 277.

LUMLEY, J. L. 1965 *Phys. Fluids* **8**, 1056.

LUMLEY, J. L. & KHAJEH-NOURI, B. 1974 *Adv. in Geophys.* A **18**, 169.

MONIN, A. S. & YAGLOM, A. M. 1971 *Statistical Fluid Mechanics*, vol. 1 (ed. J. L. Lumley) M.I.T. Press.

MONIN, A. S. & YAGLOM, A. M. 1975 *Statistical Fluid Mechanics*, vol. 2 (ed. J. L. Lumley). M.I.T. Press.

MULHEARN, P. J. & LUXTON, R. E. 1970 Experiments on uniformly sheared turbulence to large total strains. *Dept. Mech. Engng, Univ. Sydney Rep.* F–19.

MULHEARN, P. J. & LUXTON, R. E. 1975 *J. Fluid Mech.* **68**, 577.

OBOUKHOV, A. M. 1941 *Izv. Akad. Nauk S.S.S.R., Ser. geogr. geofiz.* no. 4–5, p. 453.

PRANDTL, L. 1925 *Z. angew. Math. Mech.* **5**, 136.

REIS, F. B. 1952 Ph.D. dissertation, Massachusetts Institute of Technology.

REYNOLDS, O. 1895 *Phil. Trans. Roy. Soc.* **186**, 123.

ROSE, W. G. 1966 *J. Fluid Mech.* **25**, 97.

ROSE, W. R. 1970 *J. Fluid Mech.* **44**, 767.

ROTTA, J. C. 1951 *Z. Phys.* **129**, 547; **131**, 51.

ROTTA, J. C. 1962 *Prog. in Aero. Sci.* **2**, 1.

ROTTA, J. C. 1972 *Turbulente Strömungen*. Stuttgart: Teubner.

SABOT, J. & COMTE-BELLOT, G. 1972 *C.R. Acad. Sci. Paris* A **275**, 667.

TOWNSEND, A. A. 1975 *The Structure of Turbulent Shear Flow*, 2nd edn. Cambridge University Press.

UBEROI, M. S. 1957 *J. Appl. Phys.* **28**, 1165.

WISKIND, H. K. 1962 *J. Geophys. Res.* **67**, 3033.